Department of Advanced Materials Science,

Graduate School of Frontier Sciences,

The University of Tokyo

2023

Master's Thesis

Ultra-thin film preparation of silica nanoparticles at air-water interface

気水界面におけるシリカナノ粒子からなる超薄膜形成

Submitted July 18, 2023

Supervisor: Professor Mikk Lippmaa

47-216129

張宇塵

Zhang Yuchen

Contents

Chapter 1

Introduction

1.1. Two-dimensional Materials

Two-dimensional (2D) materials refer to materials with a thickness of only a few atomic layers [1], and their crystal structure exhibits significant differences from ordinary three-dimensional (3D) materials. 2D materials have unique physical, chemical, and electronic properties, such as high surface area-to-volume ratio, high electron mobility, excellent mechanical performance, quantum confinement effect, etc. Therefore, 2D materials have gained extensive attention in the fields of nanotechnology, electronics, energy storage, and conversion [2].

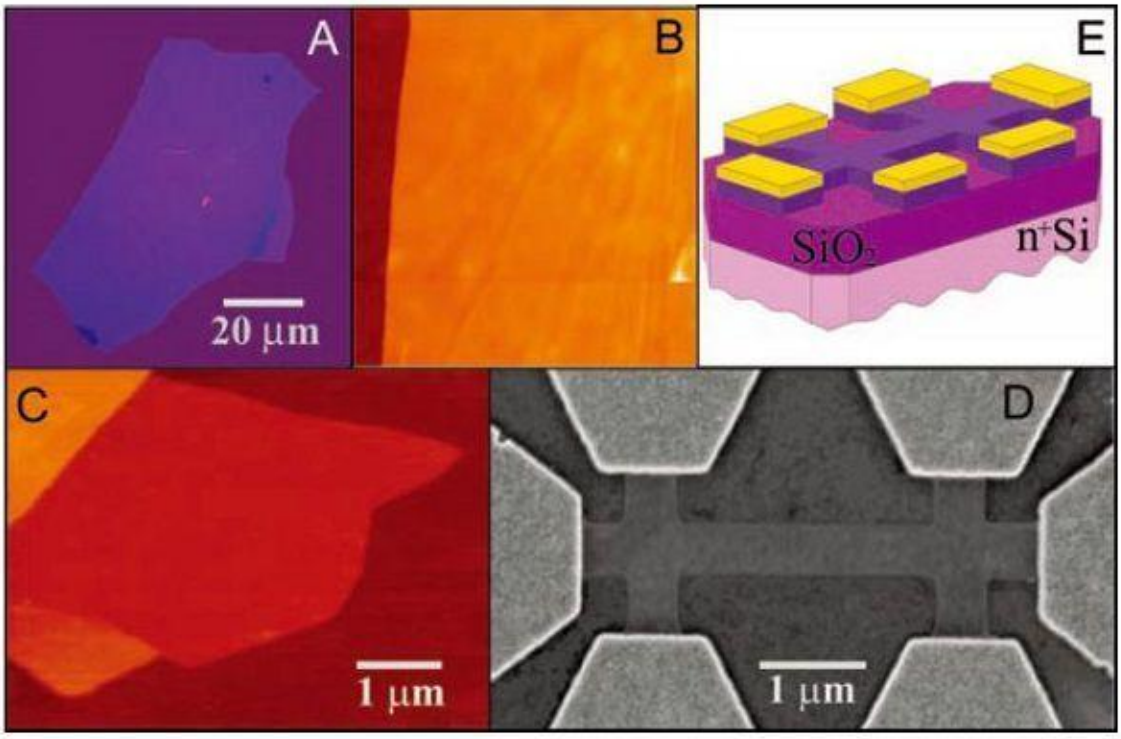

Fig. 1.1 (A) A multilayer graphene sheet with a thickness of about 3 nm; (B) AFM image near the edge of the graphene sheet; (C) AFM image of monolayer graphene; (D) SEM image of graphene film-based multi-terminal Hall Bar device; (E) Schematic diagram of graphene film-based multi-terminal Hall Bar device. [3]

Since the successful preparation of single-layer graphene by A. Geim and K. Novoselov in 2004 [3], research on 2D materials has developed rapidly. In 2006, W.A. Heer and others used standard nano-lithography techniques to grow graphene on a silicon carbide substrate [4], while K. Mullen and others discovered a method for preparing 12 nm wide 2D graphene nanoribbons [5]. Starting

with graphene, nano 2D materials have been widely studied, and many 2D materials with different structures and properties have been discovered, such as sulfides, nitrides, phosphides, carbides, and molybdenum disulfide [6]. The unique properties of these materials have made them widely used in electronics, energy, biomedical, and other fields.

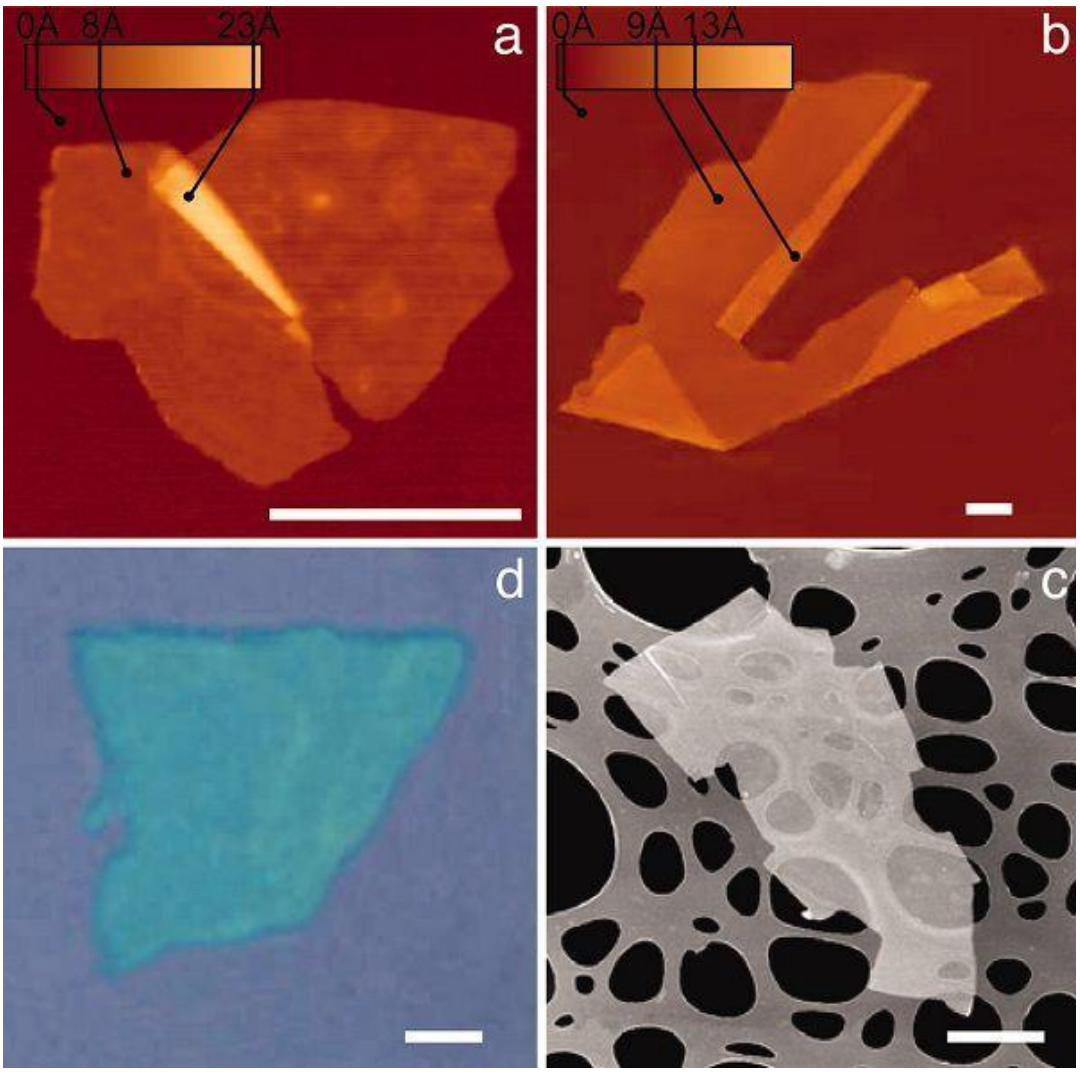

Fig. 1.2 (A) AFM image of 2D NbSe; (B) AFM image of 2D graphite; (C) SEM image of 2D $Bi_2Sr_2CaCu_2O_x$; (D) SEM image of MoS_2 (scale bar is 1 μm). [6]

In the field of electronics, 2D materials have been widely used in field-effect transistors, circuits, sensors, and other fields due to their high electron mobility and excellent mechanical performance. For example, the high electron mobility and excellent mechanical performance of graphene make it an ideal material for wearable electronic devices. In addition, 2D materials also have excellent optical properties, such as multiphoton absorption and quantum confinement effect, which can be applied in the fields of optoelectronics, nanolaser, and so on [7].

In the field of energy storage and conversion, 2D materials also have broad application prospects. For example, 2D materials such as graphene and molybdenum oxide have excellent electrochemical properties and can be used in the preparation of capacitors and batteries [8]. In addition, 2D

materials can also be used to prepare efficient photocatalysts [9], such as graphene oxide and molybdenum nitride, which can be used in the fields of photocatalytic water splitting, CO_2 reduction, and so on.

In the biomedical field, 2D materials also have broad application prospects. The high surface area-to-volume ratio and biocompatibility of 2D materials can be used in the fields of biosensing, drug delivery, and so on. For example, graphene oxide can be used to prepare efficient drug delivery carriers to achieve targeted drug delivery [10].

With the widespread application of 2D materials in various fields, research on their properties and applications is continuously deepening. 2D inorganic materials have been developed for electronic. Since the carrier migration and heat diffusion can be confined to a 2D plane [11], there is great development potential for 2D optoelectronic, thermoelectric, and bionic devices. In addition, 2D organic materials have also been developed for use in electronic devices over the past several decades [12].

However, 2D materials still have some defects in some aspects, such as mechanical stability, biocompatibility, *etc* [13]. But due to its numerous advantages that are not present in traditional materials, it is possible to combine the benefits of other materials with the excellent performance of 2D materials, thereby enhancing the overall material properties. In recent years, organic-inorganic composite materials have gradually become a research hotspot. By combining organic and inorganic materials, these materials can compensate for the defects of 2D materials while maintaining their unique properties, and open up more application fields. Therefore, exploring the preparation and performance research of organic-inorganic composite materials is of great significance for the study of 2D materials.

1.2. Organic-Inorganic Composite Materials

As a new type of material, organic-inorganic hybrid materials have received widespread attention in modern materials science due to their excellent properties and wide application prospects [14-18]. It is a new type of material composed of organic molecules and inorganic materials, the abundance of elements provides a variety of properties beyond the limits achieved using only organic and inorganic materials, making it one of the hotspots in current materials science research.

In the preparation process of organic-inorganic hybrid materials, the interaction mode and structural design between organic molecules and inorganic materials are the key to preparing high-performance composite materials. Currently, the preparation technology of organic-inorganic hybrid materials is continuously developing, and various new methods and approaches have been widely researched and applied, such as solution method, gel method, electrochemical deposition method, co-precipitation method, and pyrolysis method, which can be used to prepare high-performance organic-inorganic hybrid materials [14].

In the electronics industry, organic-inorganic hybrid materials have important applications in solar cell and microelectronic devices such as transistors and field-effect transistors [15]. By controlling the interaction between organic molecules and inorganic materials, the electrical and optical properties of the composite material can be adjusted. For example, by doping organic molecules into conductive materials, the conductivity of the material can be enhanced, and by combining inorganic materials with organic molecules, materials with excellent optical properties can be prepared [16].

In addition, organic-inorganic hybrid materials also have great advantages in material processing and preparation. Due to the interaction and molecular structural design between organic molecules and inorganic materials, the properties and performance of the material can be adjusted, and composite materials with special properties and shapes can be prepared. For example, organic-inorganic hybrid materials can be used to prepare high-strength, high-toughness, and high-heat-resistant composite materials [17]. Moreover, by assembling organic molecules and inorganic materials, composite materials with special shapes and functions, such as flexible electronic materials and biomedical materials, can be prepared [18].

In conclusion, organic-inorganic hybrid materials have broad application prospects in fields such as the electronics industry, material processing, and preparation. In the future, with the continuous development of preparation technology, organic-inorganic hybrid materials will be applied to more fields and become one of the important areas of materials science research.

1.3. POSS

1.3.1. Structure and properties of POSS

Polyhedral oligomeric silsesquioxanes (POSS) are the smallest well-defined caged silica nanoparticles with diameters ranging from 1 to 3 nm, a class of organic-inorganic hybrid compounds. Its molecular formula is $(RSiO_{3/2})_n$ (n is an even number such as 6, 8, 10, or 12), generally n=8 [19].

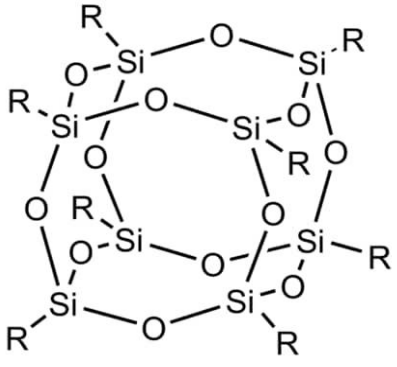

Fig. 1.3 The structure of polyhedral oligomeric silsesquioxanes (POSS).

As shown in **Fig. 1.3**, the core of the POSS molecule is a cage-like structure composed of polyhedral oligomeric silsesquioxane (POSS) units, with Si-O-Si bonds forming a tetrahedral structure around each silicon atom. This hollow and rigid cage structure gives POSS molecules excellent spatial stability, low density, low dielectric constant, and excellent optical properties. Due to the high energy of the Si-O bond compared to the C-C bond [20], as **Table. 1**, the inherent inorganic silicon-oxygen framework structure of POSS gives it excellent thermal stability, radiation resistance, and antioxidation. In addition, the distance between Si-O-Si bonds is only about 0.3 nm, giving POSS special properties at the nanoscale such as surface and interface effects, small size effects, macroscopic quantum tunneling effects, as well as quantum size effects.

Table. 1 Bond energy of several chemical bonds ($kJ \cdot mol^{-1}$).

Single bond	**H**	**C**	**N**	**O**	**F**	**Si**	**P**	**S**	**Cl**
H	436								
C	415	**331**							
N	389	293	159						
O	465	343	201	138					
F	565	486	272	184	155				
Si	320	281	-	**368**	540	197			
P	318	264	300	352	490	214	214		
S	364	289	247	-	340	226	230	264	
Cl	431	327	201	205	252	360	318	272	243

Organic groups (R groups) are attached to each silicon corner of the POSS molecule. R groups can be designed to be reactive or non-reactive, such as alkyl, alkenyl, aryl, arylene, and their derivative groups, etc. The type and quantity of organic groups can be adjusted as needed to achieve precise control of the properties of the POSS molecule.

POSS can dissolve in specific organic solvents and is easy to disperse in polymer matrices,

improving many properties of polymers, such as increasing glass-transition temperature, improving thermal decomposition temperature, improving antioxidation, reducing flammability, and reducing density.

In addition, the organic groups in POSS molecules can interact with surrounding molecules through hydrogen bonds and van der Waals forces, thereby affecting their properties and applications. Some functional groups (such as hydroxyl, carboxyl, *etc.*) in organic groups can form hydrogen bond interactions with atoms with high electronegativity (such as oxygen, nitrogen, *etc.*) in surrounding molecules or matrices, thus affecting the structural stability of POSS molecules, surface activity and wettability properties. And some larger functional groups (such as benzene rings, aromatics, *etc.*) can interact with surrounding molecules or substrates through van der Waals forces, thereby affecting the thermal stability and mechanical properties of POSS molecules.

1.3.2. Applications of POSS

This fascinating molecule between silica and polysiloxane combines the advantages of high thermal stability, chemical stability, and tunable surface chemistry of both materials and is easy to process and operate using traditional chemical techniques. Therefore, it has wide applications in many fields, including biomedical materials, luminescent materials, catalytic materials, and more.

The closed cubic silica structure exhibits a remarkably low polarity, resulting in the solubility of most hydrocarbon-substituted POSSs derivative in weakly polar organic solvents, such as chloroform, tetrahydrofuran, and occasionally hexane. However, when polar functional groups are introduced at the vertices, POSS becomes soluble in polar solvents such as water and methanol while still maintaining the hydrophobic spaces surrounding the silica cube [21]. This intriguing property of POSS, known as amphiphilicity, arises from the weak polarity of the closed silica cage when immersed in water. The hydrophobic nature of POSS serves as a driving force for robust interactions with hydrophobic molecules, enabling their encapsulation within POSS-based materials in aqueous environments, as shown in **Fig. 1.4**.

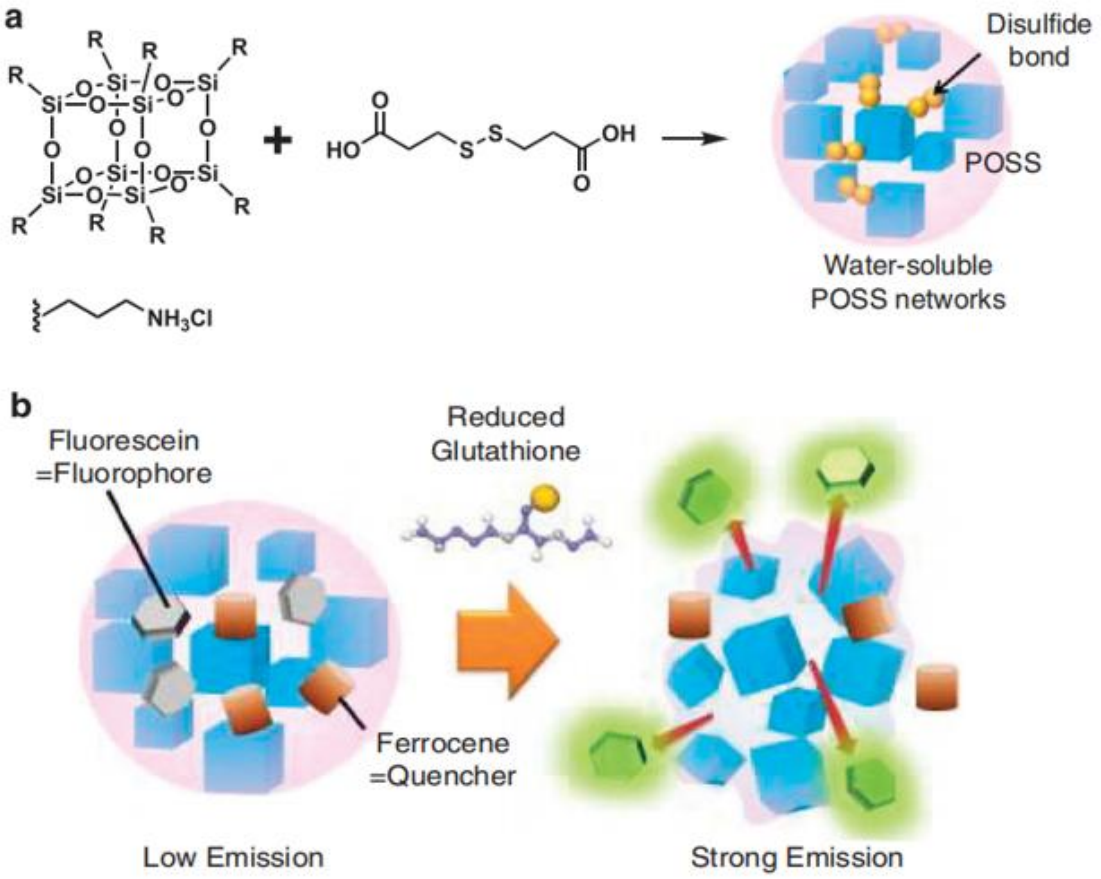

Fig. 1.4 (a) Creation of strong hydrophobic spaces inside the water-soluble POSS network polymers with disulfide bonds. (b) The encapsulated fluorophores (fluorescein) are released by adding glutathione. Subsequently, the fluorescence emission is recovered. [21]

POSS-based nanomaterials can increase surface energy in the silicon-rich region, making them highly biocompatible and therefore more suitable for use in biomedical materials such as drug delivery, gene carriers, biomedical devices, tissue engineering scaffolds, and dental materials. Due to its small size and high payload capacity, POSS exhibits high transportability and can improve the uptake rate of biological tissues. As shown in **Fig. 1.5**, functional micelles can be prepared by using POSS hybrid materials with polymer chains to encapsulate drugs in a hybrid polymer system through self-assembly technology to achieve controlled drug release in the human body [22]. Due to its good biocompatibility, the synthesized hybrid polymer material can undergo biodegradation and be eliminated from the human body after drug release; and the POSS core greatly improves the thermal stability of the self-assembled material, which can prolong the circulation time of polymer nanomicelles in the body.

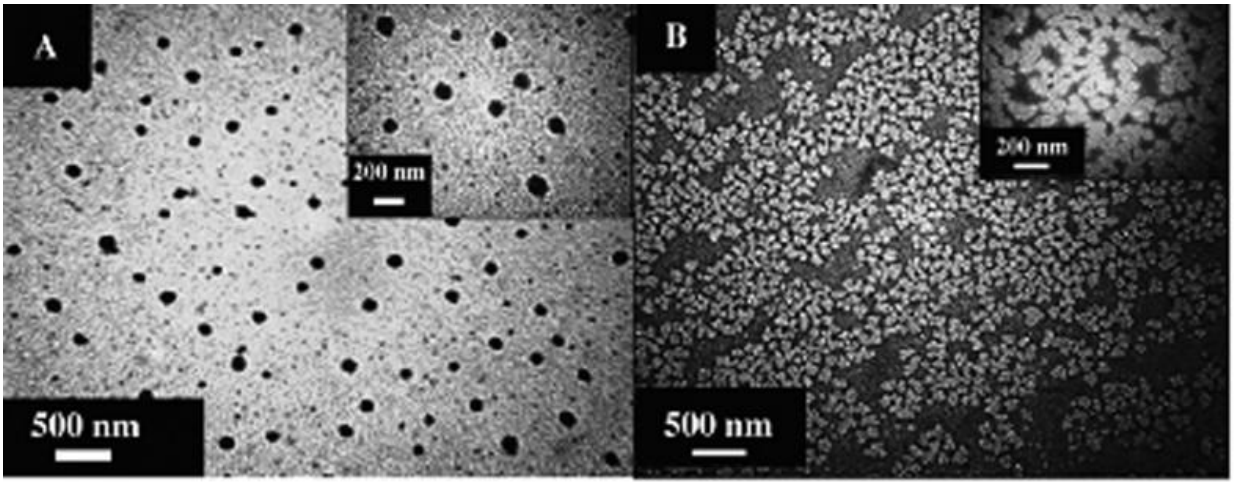

Fig. 1.5 BIO-TEM images of POSS-g-PVA NPs: (A) before drug loading and (B) after drug loading. [22]

Research on POSS-based luminescent materials has also been a hot topic in recent years. In principle, a combination of two or three different colors is necessary to produce white light. Typically, in dye mixture materials, it is easy to change the color balance of displaying white light by heating because each emission characteristic is sensitive to environmental changes and will degrade independently. The introduction of POSS into the mixed material achieves dual emission characteristics, emitting white light composed of blue and orange emissions [23], as shown in **Fig. 1.6**. Due to the good compatibility between POSS and conjugated polymers, these color balances can be maintained even in high-temperature regions. Therefore, a hybrid film with thermally stable white light emission can be obtained through simple mixing and painting procedures.

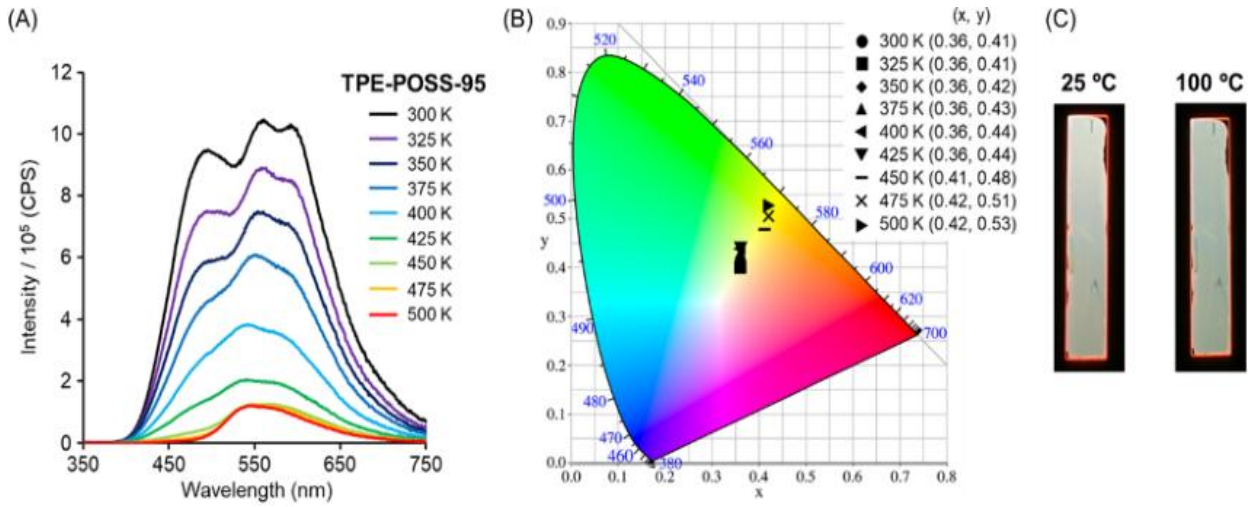

Fig. 1.6 (A) Variable temperature (VT) PL spectra, (B) CIE diagram, and (C) photographs under heating [excited by a UV lamp (365 nm)] of TPE-POSS-95. [23]

1.4. Inorganic materials as substrates

Preparing POSS molecules into 2D materials and transferring them onto solid substrates to form composite materials has become a highly regarded research direction, offering new properties and potential applications to the materials. In this process, the selection of suitable solid substrates is crucial for the final performance and application potential of the composite material. The selection of solid substrates needs to consider several aspects, including their properties, compatibility, interface interactions, and anticipated application requirements, in order to achieve optimal composite material performance and application potential.

1.4.1. Considerations for selecting solid substrates

Firstly, the properties of the solid substrates play a significant role in the performance of the composite material. For instance, in optical sensor applications, transparency and optical transmittance are critical considerations, making glass substrates a common choice. For electrical or magnetic sensors, solid substrates with good conductivity or magnetism, such as silicon substrates or magnetic materials, can be selected.

Secondly, compatibility between the solid substrates and POSS molecules is of utmost importance. Compatibility affects the adsorption and binding capacity of POSS molecules on the substrate surface, directly influencing the structure and stability of the composite material. Choosing a substrate with better compatibility can enhance the interaction between POSS molecules and the substrate, facilitating molecular assembly and film stability.

Furthermore, interface interactions are also a significant aspect of solid substrate selection. Interface interactions involve factors such as interfacial energy, adhesion force, and interface structure, which have a crucial impact on the mechanical properties of the composite material and the stability of the interface. Therefore, when selecting a solid substrate, the interface interactions with POSS molecules need to be considered to achieve good interfacial bonding and mechanical performance.

Lastly, anticipated application requirements also influence the selection of solid substrates. Different application fields have varied demands for composite materials. For example, in sensors, the chemical stability, heat resistance, and responsiveness to target molecules or environmental factors of the substrate need to be considered.

1.4.2 Transfer methods and applications for different substrates

Thermo-compression bonding is a technique used to create a bond between two materials by applying heat and pressure [24]. It is commonly employed in microelectronics and semiconductor

industries for joining two substrates or components together. The process involves placing the materials in contact, applying controlled heat to raise their temperature, and simultaneously applying pressure to promote interatomic bonding between the surfaces. This bonding method is particularly useful for achieving strong and reliable bonds between materials with compatible melting temperatures.

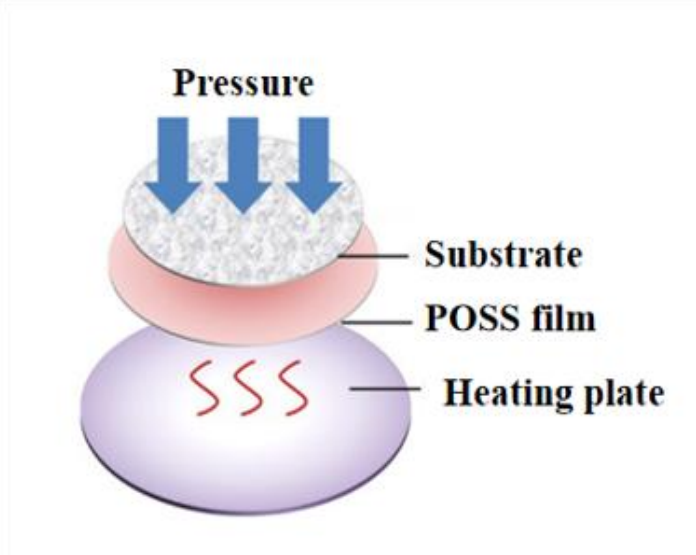

Fig. 1.7 Schematic diagram of the principle of the Thermo-compression bonding method.

The solvent transfer method is a technique used to transfer a thin film or layer from a donor substrate to a receiving substrate using a solvent as a carrier. The process typically involves depositing the film on the donor substrate, followed by the application of a solvent that selectively dissolves the interface between the film and the donor substrate. As a result, the film is delaminated or detached from the donor substrate and floats on the solvent's surface. The receiving substrate is then brought into contact with the floating film, allowing it to be transferred onto the new substrate. This method is often employed when the film exhibits poor adhesion to the original substrate or when a flexible or fragile film needs to be transferred without damage. Among them, the spin coating method is the most well-known solvent transfer methods. The basic principle of the spin coating method is to place the solution on the rotating substrate and distribute it evenly on the surface of the substrate through the force of rotation to form a thin film [25], as shown in **Fig. 1.8**. It has the advantages of simple operation, high uniformity of thin film coating, rapid preparation, and application to various materials.

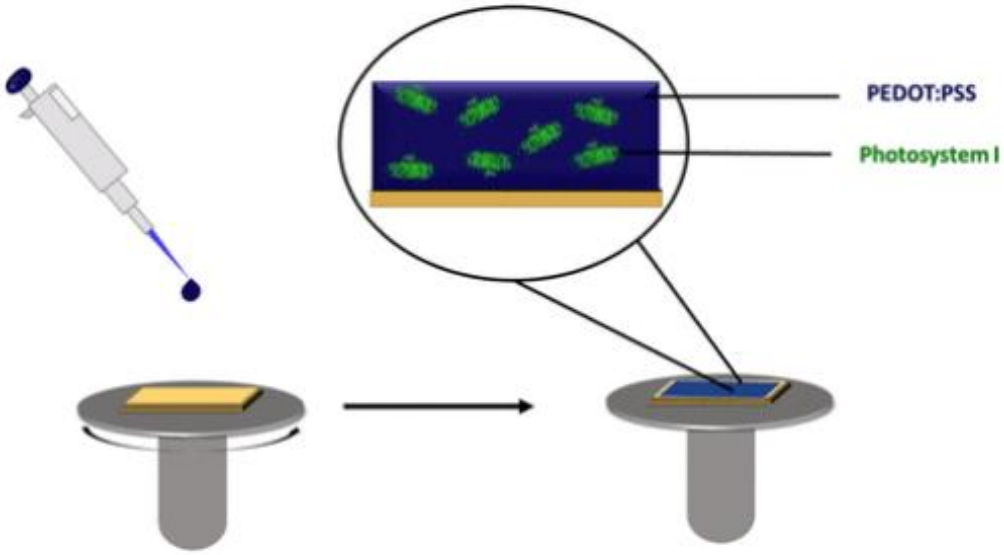

Fig. 1.8 Schematic diagram of the preparation of photosensitive composite film by spin coating method. [25]

When selecting solid substrates, there are various options to consider, including silicon, glass, ceramics, metals, and more. Common transfer methods include the thermo-compression bonding, and solvent transfer method. For silicon substrates, when POSS film combines with the silicon wafer, it can form a strong interface due to the reactive nature of the silicon surface, allowing for chemical bonding or physical adsorption with the POSS film [26]. This interface bonding provides higher mechanical strength and thermal stability, resulting in good adhesion and durability of the POSS film on silicon-based materials. Additionally, POSS films can improve the surface properties of silicon substrates. For example, silicon surfaces typically have poor wettability, but by forming a POSS film on the silicon surface, the wetting performance can be significantly enhanced, making the surface more conducive to the spreading and uniform distribution of liquids. This is particularly beneficial for applications involving coating or liquid transfer. Furthermore, POSS films can provide additional chemical stability, enhancing the corrosion resistance and resistance to chemical attack of silicon substrates.

For glass substrates, POSS films have a wide range of applications. When transferred onto the glass surface, POSS films can form uniform and smooth coatings [27]. These coatings exhibit excellent optical properties, such as low reflectivity and high transmittance, making them suitable for producing anti-reflection coatings that improve the efficiency and clarity of optical devices. Additionally, POSS films possess outstanding durability and chemical stability, offering protection to glass substrates against environmental damage. This makes POSS films highly promising for applications in sensors, display devices, and optical coatings, among other fields.

Both silicon substrate and glass substrates are well-suited for the transfer of POSS. However, compared to silicon and glass, other substrates may have certain drawbacks to varying degrees. For

example, in the case of ceramic substrates, although the transferred POSS film can provide wear resistance, corrosion resistance, and high-temperature stability to the ceramic surface, the unique characteristics of ceramic materials may require higher temperatures, pressures, and specialized surface treatment methods during the transfer process of the POSS film [28]. Additionally, the chemical composition and crystal structure of ceramic materials can also affect the transfer properties of POSS films. And as for metal substrates, POSS films can improve their surface properties, such as enhancing corrosion resistance, hardness, and wear resistance [29]. However, a disadvantage is that during the transfer process, insufficient bonding strength may be encountered, which may require surface treatment or the use of appropriate interface layers to enhance the adhesion between the film and the metal substrate.

1.5. Outline of this thesis

In summary, considering the cost and other factors, selecting glass substrates as the foundation for POSS composite materials is a wise choice that can provide excellent performance and potential prospects for sensing applications. Langmuir-Blodgett (LB) method is a commonly used technique for preparing ordered thin films on solid surfaces. It is applicable to many materials, including POSS [30]. There are several reasons for choosing the LB method to transfer POSS onto a glass substrate.

Firstly, the ordered nature of the films. The LB method allows for the preparation of highly ordered thin films on solid surfaces. During the LB process, POSS molecules form a monolayer at the interface and undergo compression, stretching, or tilting to arrange and orient themselves. This ordered molecular arrangement provides precise structural control.

Secondly, control over monolayer thickness. The LB method enables the fabrication of thin films with a monolayer thickness. This is particularly important for applications such as nanodevice fabrication in optics, electronics, and sensors. Monolayer thin films of POSS molecules offer highly controllable nano-scale structures.

Thirdly, surface modification and functionalization. By transferring POSS onto a glass substrate using the LB method, it becomes possible to modify and functionalize the glass surface. POSS molecules possess various functional groups that can chemically react or interact with the substrate surface. This allows for the introduction of new properties and functionalities to the glass surface, such as enhanced wettability, improved corrosion resistance, or increased optical characteristics.

Lastly, the construction of multilayer thin films. The LB method allows for the construction of multilayer thin film structures, where the arrangement and properties of each layer can be precisely controlled. Through repeated deposition and transfer steps, complex multilayer structures can be formed, enabling more sophisticated functionalities and performances.

In conclusion, the choice of using the LB method to transfer POSS onto a glass substrate is

motivated by its advantages in providing orderliness, control over monolayer thickness, surface modification, and construction of multilayer structures. These advantages contribute to achieving the desired material properties and functionalities. Regarding the LB method, I will introduce it in detail in the next chapter.

Chapter 2

Methods

2.1 Langmuir-Blodgett trough

The core method employed in this research is the Langmuir-Blodgett (LB) method, which was originally designed and developed by I. Langmuir and K. Blodgett [31]. The LB method is one of the most well-known and extensively validated techniques for layer-by-layer molecular thin film fabrication.

The LB process of molecular monolayer formation is done in a Langmuir trough, which consists of the trough and one or two barriers [32], as shown in **Fig. 2.1**. The trough surface may be covered with a superhydrophobic coating or, as was done in this work, the trough was machined out of a block of polytetrafluoroethylene (PTFE).

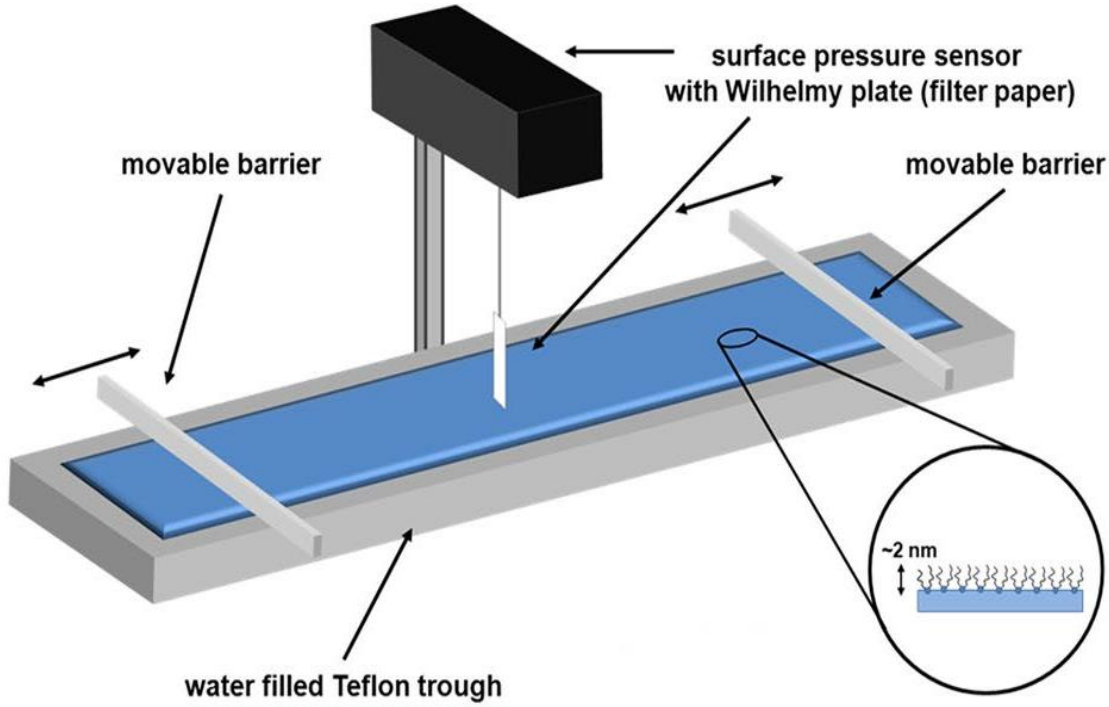

Fig. 2.1 Schematic illustration of the LB trough system. [32]

The liquid present in the trough is referred to as the subphase. The subphase is typically water, although various organic solvents may also be used to accommodate the surface-active molecules. The properties of the subphase, such as pH and temperature, can influence the behavior and arrangement of the surface-active molecules. After spreading the molecules on the subphase, in order to control the arrangement of the molecules and the quality of the film, one or two barriers that form a meniscus with the subphase liquid are slowly moved closer to each other. The subphase

meniscus at the barriers keeps the molecules at the subphase surface between the barriers, compressing the molecules at the surface in the restricted region between the barriers. In an ideal case, the molecules may then form an ordered monolayer, commonly known as the Langmuir monolayer [33], although various molecular clusters or other larger structures may also form. As shown in **Fig. 2.2**, the surface pressure of the molecular layer is measured by contacting the subphase surface with a Wilhelmy plate and measuring the force exerted by the liquid on the plate. The measured force can be converted to the surface tension of the liquid, which is used to record the compression and film formation process [34]. In this approach, the estimation of surface tension γ is based on the application of a drawing force mg to a thin plate submerged in a subphase until the meniscus contacts the subphase surface. The expression for surface tension γ is as follows;

$$\gamma = \frac{mg}{2(L+L_0)} ,$$

where L and L_0 are noted in **Fig. 2.2**. While the surface pressure, π, is typically expressed as the difference between surface tension of pure water (γ_0) and the molecular monolayer (γ);

$$\pi = \gamma_0 - \gamma .$$

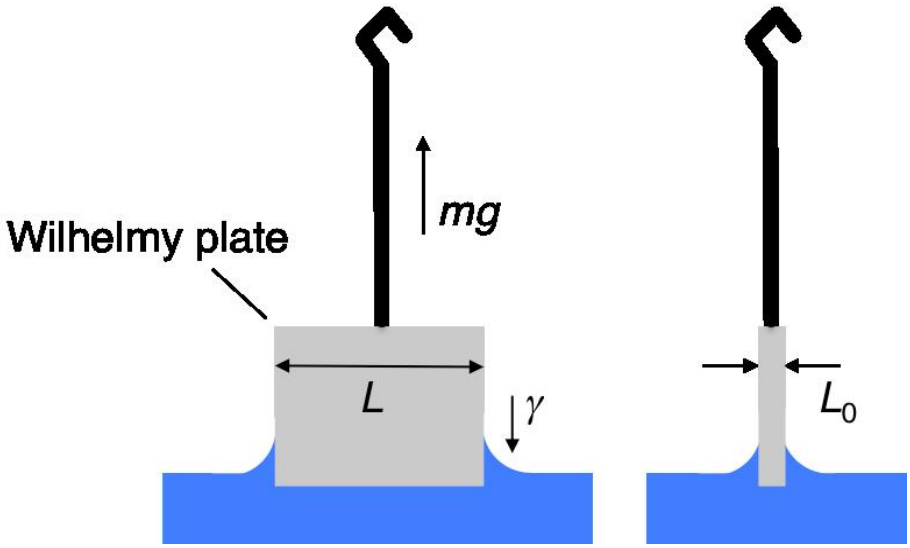

Fig. 2.2 Schematic diagram depicting the application of the Wilhelmy plate for measuring surface tension. [34]

The LB technique is a method used to prepare thin films with specific molecular arrangements, and its fundamental principle lies in the self-assembly characteristics of molecules at the air-water interface. To achieve this purpose, it is necessary to design amphiphilic molecules with appropriate polar (hydrophilic) and/or non-polar (hydrophobic) substituents. Essentially, in amphiphilic

molecules, hydrophilic substituents are located at the air-water interface. While hydrophobic substituents such as alkyl chains remain standing in the air phase. As shown in **Fig. 2.3**, stearic acid is a traditional amphiphile. By controlling the compression and transfer of these molecules, they are transferred onto a solid substrate.

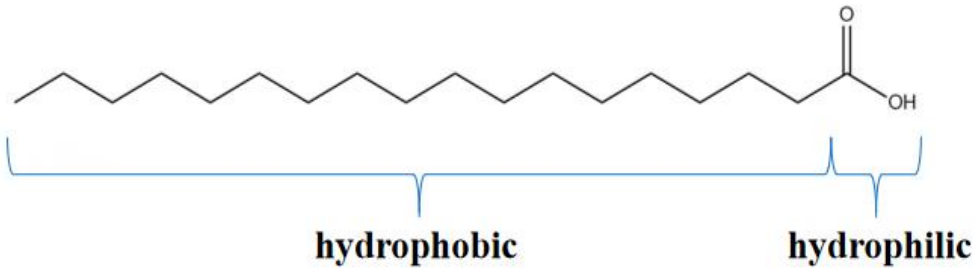

Fig. 2.3 Structural formula of the amphiphilic stearic acid ($C_{18}H_{36}O_2$).

Langmuir films prepared through LB technique possess numerous advantages. Firstly, Langmuir films exhibit highly ordered molecular arrangements, which can control dense packing of molecules and achieving directional molecular organization. Secondly, the thickness of the Langmuir film can be precisely controlled, and it exhibit uniformity and density. These characteristics make Langmuir films widely applicable in fields such as optoelectronics, sensors, coatings, catalysts, and more.

Furthermore, LB technique enables the fabrication of multilayered thin films [35]. By stacking different molecular layers, more complex functionalities and properties can be achieved. For example, by layering molecules with distinct properties or functionalities, it is possible to construct multifunctional thin films with specific optical, electrical, or chemical responses.

In summary, Langmuir-Blodgett technology is an important thin film fabrication technique. By precisely controlling the organization and arrangement of molecules, thin film materials with specific functions and properties can be prepared, finding extensive applications in materials science, nanotechnology, and related fields of research and application.

2.2 *π-A* isotherm

In the LB technique, by recording the surface area and the corresponding surface pressure values, a surface pressure-area curve, also known as surface pressure-area (π-A) isotherm, can be obtained.

A representative surface pressure-area (π-A) isotherm is illustrated in **Fig. 2.4** [33, 34]. As the molecular area A decreases, the surface pressure π gradually increases. The physical state of the monolayer is influenced by the interactions among the molecules in the surface layer, where the force and range of interactions change as the molecules approach each other. Accompanied by phase transitions of the spreading 2D monolayer, there are some analogies to three-dimensional materials. **Fig. 2.4** is a typical schematic illustration, and the actual experimental π-A curve heavily depends on the spreading of organic materials.

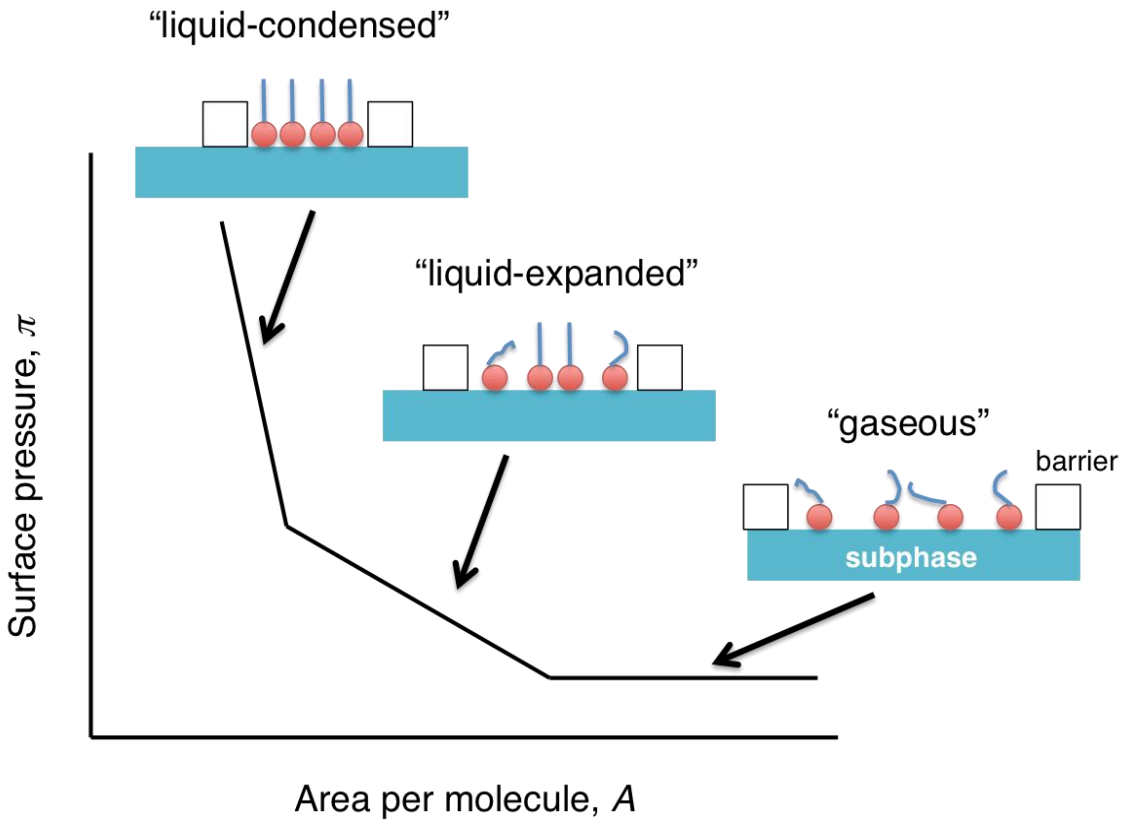

Fig. 2.4 A representative isotherm depicting the relationship between surface pressure and area (π-A) is presented, featuring distinct phase transitions. Additionally, a schematic representation of the molecular state on the subphase is provided for each phase. [33, 34]

Particular orientation and arrangement of molecules on the subphase surface correspond to specific states. **Fig. 2.5** illustrates various potential phase states achievable by compressing monolayers [36, 37, 38]. In the case of a large area, the highly decompressed monolayers formed after applying the solution can be observed as 2D gaseous (G). As the molecules approach each other within the monolayer, their interactions intensify, resulting in an increase in surface pressure. This indicates the transition from the gas phase (G) to the liquid-expanded phase (LE). This transition takes place across a broad coexistence region, wherein both phases present simultaneously. Further compression induces a phase transition from the liquid-expanded phase (LE) to the liquid-condensed phase (LC), characterized by the emergence of structural coherence within a short range. This transition is typically observed as a region with constant pressure (referred to as a plateau) on isotherms and is known as a first-order phase transition (π_{pt}). In the case of a first-order phase transition, the slope of the isotherm becomes zero. In addition, certain materials such as stearic acid, the compressed monolayer exhibits a significant increase in pressure, leading to its transition into the solid phase (S). When the surface pressure reaches a significantly higher level, the monolayer eventually undergoes collapse [39].

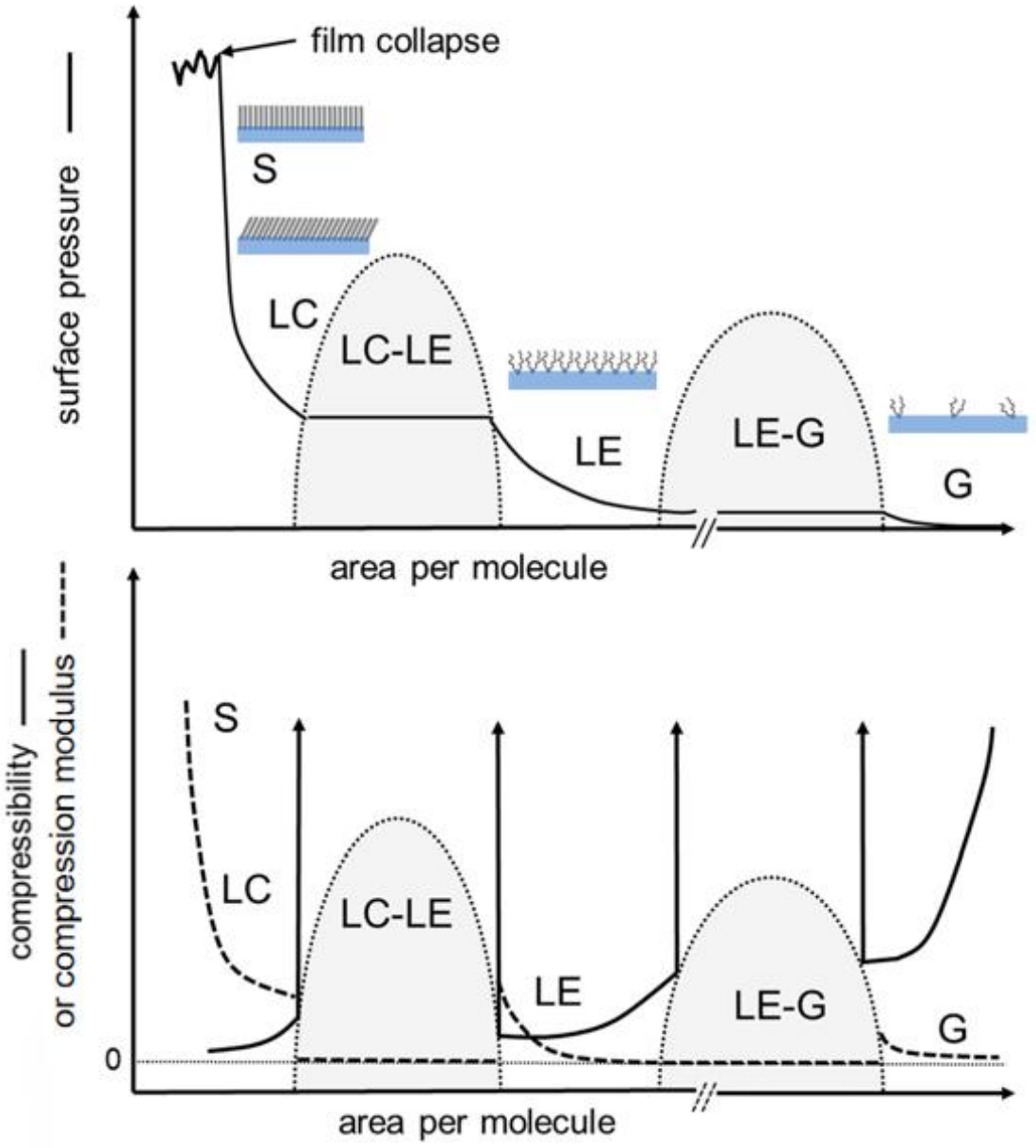

Fig. 2.5 Top: Schematic illustration depicting an isotherm of a Langmuir monolayer. The Langmuir monolayer exhibits various phases, namely the G phase indicating gas-analog state, the LE phase indicating liquid-expanded state, the LC phase indicating liquid-condensed state, and the S phase indicating solid-analog state. The regions shaded in gray indicate the coexistence of two distinct monolayer phases.
Bottom: Schematic illustration of the compressibility C_s and the compression modulus C_s^{-1} in relation to the molecular area. The C_s values theoretically approach infinity during the LC–LE and LE–G phase transitions regions, while C_s^{-1} tends to zero. However, experimental isotherms in the phase transition region exhibit finite slopes, indicating that C_s does not actually reach infinity. [36, 37, 38]

Additionally, the compression isotherms (π-A) can be used to identify two significant parameters: the lift off area (A_0) and the limit area (A_{lim}). The parameter A_0 signifies the critical area where the

transition from the gaseous phase to the expanded liquid phase takes place, marking the onset of the isotherm's ascent. Conversely, the limit area plays a crucial role in determining the area occupied by each molecule within a densely packed monolayer. It is derived by extrapolating the linear segment of the isotherm to a surface pressure value of zero ($\pi = 0$). By comparing these parameters with the molecular cross-sectional area, useful information on the state of the molecular layers can be obtained.

To investigate surface pressure-area isotherms, it can be beneficial to examine the isothermal compressibility C_s or the compression modulus C_s^{-1} of a monolayer in relation to surface pressure or molecular area [40]. The compressibility C_s can be defined as follows;

$$C_s = -\frac{1}{A}\left(\frac{dA}{d\pi}\right)_{n,T} \quad .$$

The compression modulus, which is a measure of how condensed a monolayer is, is obtained from the numerical data of the *π-A* isotherms with the help of the formula shown below

$$C_s^{-1} = -A\left(\frac{d\pi}{dA}\right)_{n,\,T} \quad ,$$

where: *A*—area per molecule, *π*—surface pressure, *n*—number of moles, *T*—temperature.

The compression modulus characterizes the mechanical stiffness of the monolayer [41] and can be used to determine which phase corresponds to monolayer. For instance, a liquid expanded monolayer has a low compression modulus of less than 50 mN/m, a liquid-condensed layer falls in the range 100-250 mN/m, and a solid monolayer has a modulus above 250 mN/m.

The bottom part of **Fig. 2.5** depicts a diagram illustrating the relationship between C_s and C_s^{-1} with respect to the molecular area. It is worth noting that in many instances, C_s and C_s^{-1} are presented as a function of surface pressure rather than molecular area. Both C_s and C_s^{-1} demonstrate discontinuities within the phase transition range, with C_s tending towards infinity and C_s^{-1} approaching zero. The isotherm shown in **Fig. 2.5** is an illustration of what might be observed in a measurement when multiple phases occur at different stages of layer compression. In actual systems, the slope in the coexistence region between LC and LE is not zero but finite, and the onset of the phase transition is usually not as sudden as depicted in the schematic diagram.

π-A isotherms provide information about the structure and arrangement of molecules at the liquid surface. By analyzing the features of the curve, it is possible to determine the molecular assembly, layer stacking, and morphological transitions. By adjusting the solution concentration, compression rate, and compression degree, the shape of the *π-A* isotherm can be modified. Such variations can

help determine the stability of the film under different temperatures, compression degrees, and environmental conditions, thus aiding in the optimization of the film preparation process.

2.3 Transfer process

To fabricate a LB film, the process involves transferring the Langmuir monolayer onto a solid substrate under specific surface pressure conditions. This transfer is accomplished using a vertical lifting technique. In this method, the substrate is either lifted out of or immersed into the subphase, with its surface plane positioned perpendicular to the surface of the subphase, as shown in **Fig. 2.6**. To facilitate a more effective transfer, it is essential to ensure that the substrate's surface is appropriately modified to be hydrophilic or hydrophobic.

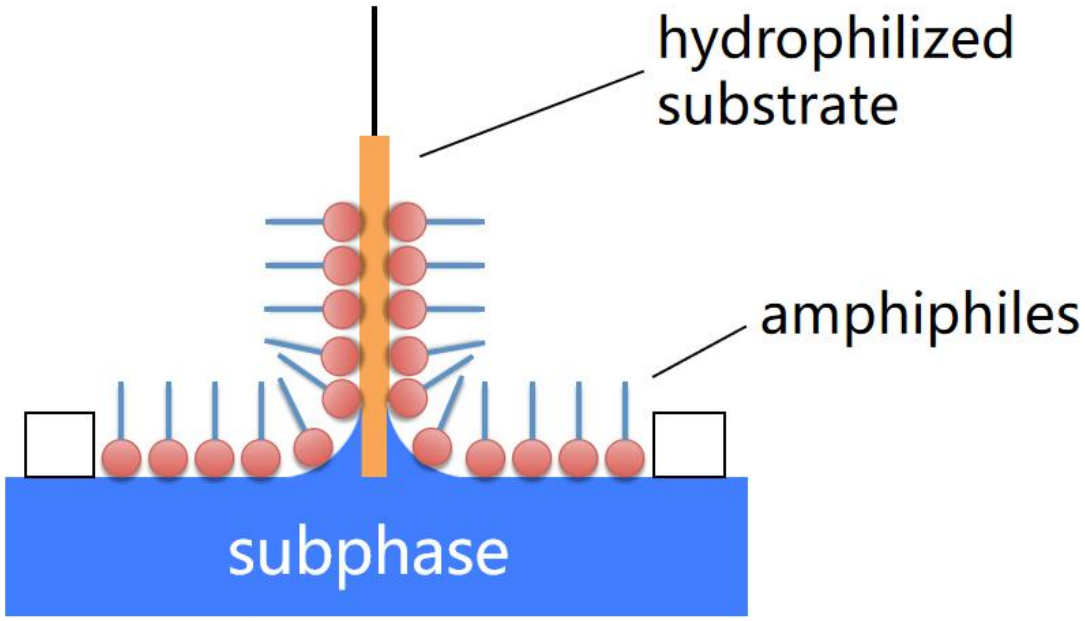

Fig. 2.6 Schematic illustration of the vertical lifting method for transfer of Langmuir monolayer. (At this point the surface of the substrate is hydrophilic.)

During the transfer process, the molecules within the Langmuir monolayer undergo changes in their orientation, influenced by both the hydrophilicity/hydrophobicity of the substrate and the direction in which the substrate moves. A hydrophilic substrate encourages stronger interactions with hydrophilic molecules, facilitating their preferential orientation and alignment. On the other hand, a hydrophobic substrate favors interactions with hydrophobic molecules, leading to their specific arrangement within the film.

Furthermore, the movement direction of the substrate during transfer also impacts the molecular organization within the Langmuir monolayer. As the substrate is lifted or dipped into the subphase, it exerts forces on the monolayer, causing changes in the packing and alignment of the molecules.

This dynamic process allows for control over the molecular orientation and ordering within the film, which can have a significant impact on the film's properties and functionality.

In addition to the traditional vertical lifting method, another technique known as horizontal lifting can also be employed for transferring the Langmuir monolayer, as illustrated in **Fig. 2.7**, this method is called Langmuir-Schaefer method [42]. In this case, the hydrophobidized surface of the substrate proves to be appropriate. This is due to the arrangement of amphiphilic molecules at the subphase surface, wherein their hydrophobic groups are exposed to the air phase. This orientation is driven by the desire to minimize contact between the hydrophobic regions and the surrounding aqueous subphase.

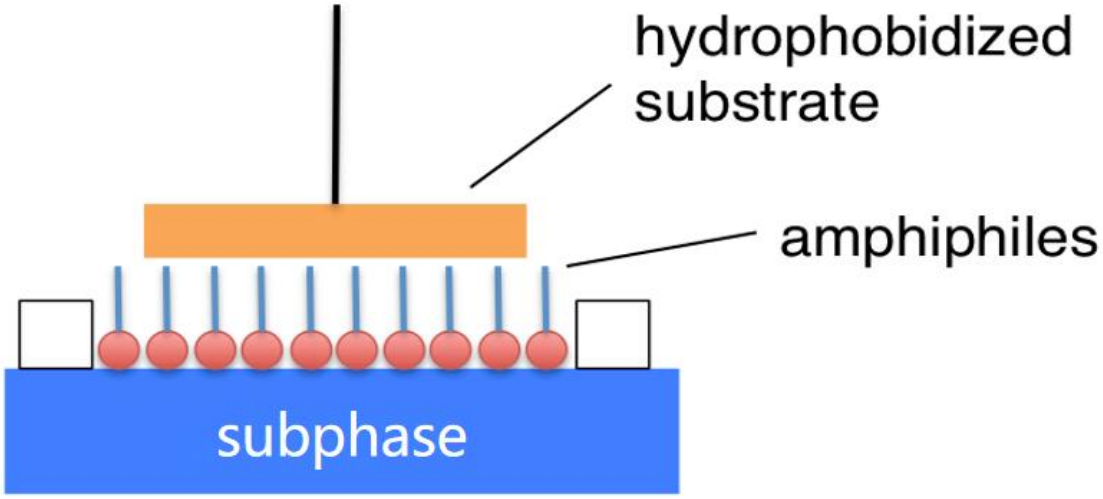

Fig. 2.7 Schematic illustration of the horizontal lifting method employed in the transfer of Langmuir monolayer.

Langmuir-Schaefer method provides an alternative strategy to regulate the arrangement and orientation of the Langmuir monolayer during the transfer process. The hydrophobic nature of the substrate allows for stronger interactions with the hydrophobic segments of the amphiphilic molecules. As a result, during the transfer process, the Langmuir monolayer undergoes reorganization to align its hydrophobic regions towards the hydrophobized substrate surface. This alignment and reorientation influence the final structure and properties of the film. The film transferred at this time is called Langmuir-Schaefer film.

The transfer of the Langmuir monolayer onto a solid substrate is a crucial step in the LB method. When the transfer is conducted only once, a monolayer can be obtained, which refers to an extremely thin layer. Precisely controlled multilayer films can also be formed by repeating the transfer process multiple times, each time adding a new monolayer on top of an existing film, to achieve the desired thickness and complexity of the multilayer structure.

Chapter 3

Experiment

3.1. Materials

Nine different types of POSSs were used in this experiment. They are divided into three categories according to the substituents to better differentiate them. The first category consists of POSSs molecules with eight identical substituent groups (**Table. 2**). The second category consists of POSSs molecules with one long-chain substituent, typically with hydrophilic functional groups, and the remaining seven substituents are isopropyl groups (**Table. 3**). The third category comprises special semi-cage-like structures of POSS (**Table. 4**). All POSSs were purchased from Merck, Sigma-Aldrich.

Table. 2 The first category of POSSs, with eight identical substituents.

	Name	Structure	Molecular Weight
POSS-1	PSS-Octamethyl substituted	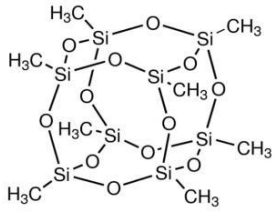	536.95
POSS-2	PSS-Octaphenyl substituted	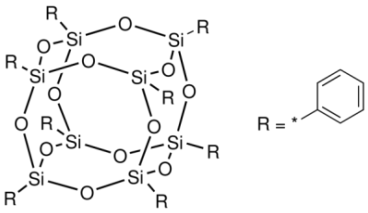	1033.51
POSS-3	PSS-Octacyclohexyl substituted	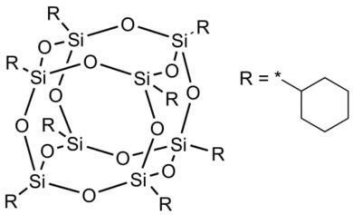	1081.89
POSS-4	PSS-Octakis(dimethylsilyl oxy) substituted	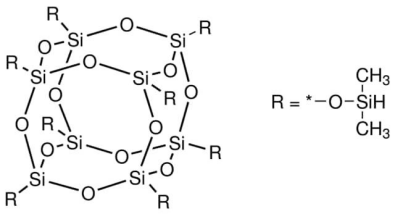	1017.97

Table. 3 The second category of POSSs, with one long chain substituent. The long chain usually has a hydrophilic functional group, and the remaining seven substituents are isopropyl groups.

	Name	Structure	Molecular Weight
POSS-5	PSS-[3-(2-aminoethyl) amino]propyl-heptaisobutyl substituent	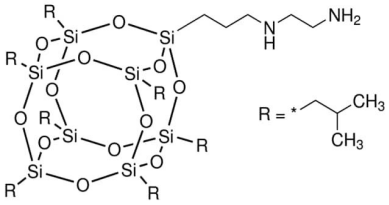	917.65
POSS-6	PSS-(2-(trans-3,4-Cyclohexanediol)ethyl)-heptaisobutyl substituted	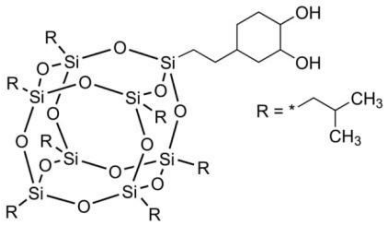	959.68
POSS-7	PSS-(2,3-Propanediol)propoxy-heptaisobutyl substituted	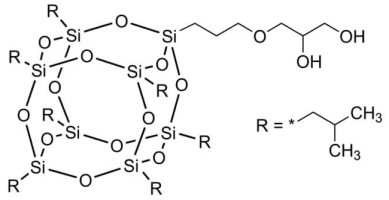	949.64
POSS-8	PSS-(1-Propylmethacrylate)-heptaisobutyl substituted	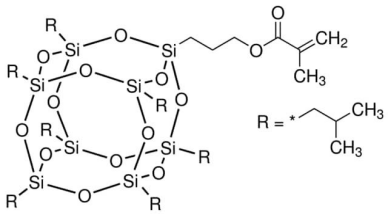	943.64

Table. 4 The third category of POSS, with only seven silicon atoms, has a special semi-cage structure, called incompletely condensed POSS (IC-POSS). Since each substituent of the following POSS is isooctyl group, the overall molecular size is very large.

	Name	Structure	Molecular Weight
POSS-9	PSS-Trisilanol-isooctyl substituted	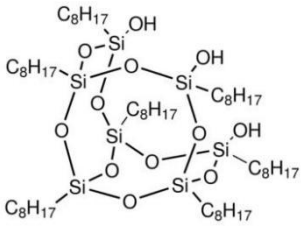	1184.16

Among them, the POSS shown in **Table. 4** is called incompletely condensed POSS (IC-POSS),

which is partially hydrolyzed from a completely condensed POSS (CC-POSS) analogue [43, 44]. The melting point (-18 °C) of this isooctyl-substituted IC-POSS is much lower than that of other POSSs. It is in liquid form at room temperature, whereas other POSSs are in solid form.

In order to obtain a Langmuir monolayer on a subphase, the target molecules first need to be dissolved in an organic solvent that does not normally react with or dissolve in the subphase. Considering the volatility, spectroscopic grade chloroform is used as a solvent with a purity of over 99.0%, purchased from Dojindo, Co.

Before the experiment, the inner surface of the LB trough needs to be cleaned to remove any possible contaminants. Considering both cleanliness and volatility, acetone is used for the cleaning purposes, purchased from FUJIFILM Wako Pure Chemical Co.

For film transfer experiments, microscope slide cover glass was used, with each piece measuring 18 mm × 18 mm, purchased from Matsunami-glass, Co. (Osaka, Japan). The cover glass plates were cut into a size of 18 mm × 9 mm using a diamond knife, which is convenient for immersion in the subphase after fixation and subsequent measurement after transfer. After cutting the glass substrate, the slices were placed in a beaker containing acetone, and washed in an ultrasonic cleaner for 5 min. After the first washing step, the substrates were moved to another beaker for secondary cleaning, repeating the ultrasonic wash for 5 min, and finally dried for later use.

3.2. Equipments

The ideal π-A isotherm is independent of the size of the LB trough. In reality, however, POSS molecules may aggregated at the air-water interface due to limited trough surface area, which means that the final π-A isotherm may still be affected by the size of the LB trough. Therefore it is necessary to use different sizes of LB troughs for comparison.

Four different-sized LB troughs were used, two from our lab, fabricated by ourselves, named LL 1 (250 mm × 80 mm) and LL 2 (440 mm × 130 mm), and the other two from National Institute for Materials Science (NIMS), Ariga laboratory, purchased from USI Co. Ltd, named NIMS 1 (334 mm × 100 mm) and NIMS 2 (544 mm × 150 mm). Since the two LB systems in our lab were self-made, their performance had to be compared with commercial LB systems. These LB troughs, as shown in **Fig. 3.1**, have different widths. The barriers pass across the water surface at the same compression speed (0.1 mm/s), and the compressed area, that is, the molecular area reduced per second is different, which directly affects the π-A isotherm.

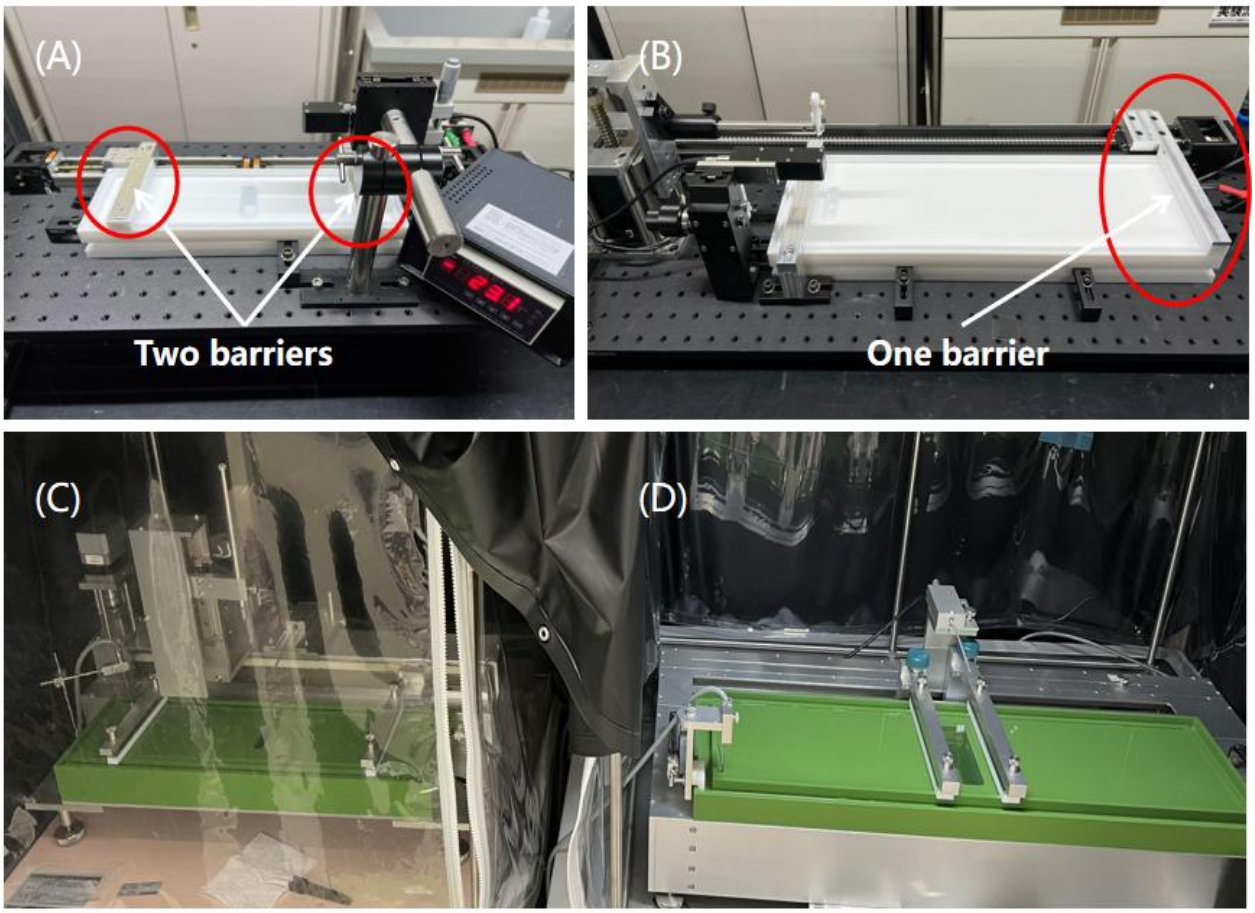

Fig. 3.1 (A) LL 1 with two barriers, 250 mm × 80 mm in size. (B) LL 2 with one barrier, 440 mm × 130 mm in size. This is an improved version, which will be described in Chapter 4. (C) NIMS 1 with two barriers, 334 mm × 100 mm in size. (D) NIMS 2 with two barriers, 544 mm × 150 mm in size.

Among them, LL 1 and the two from NIMS have two barriers. Additionally, their grooves, where the solid substrate is pre-immersed, are positioned in the middle of the trough. On the other hand, LL 2 (**Fig. 3.1 (B)**) has only one moving barrier, and the transfer pocket is positioned at the end of the trough, , close to the immobile barrier.

For the two LB troughs in our lab, the target distance, compression speed, holding pressure, dipping speed, etc. can all be controlled through the LB controller on a tablet PC, as shown in **Fig. 3.2**, and the compression distance, dipping distance, surface pressure-length curve are also displayed in a browser. The holding pressure will be introduced in detail in Section 3.3.3. Although the surface pressure-length curve is not equivalent to the π-A isotherm, the shape of the curve is similar, so it can be judged during the experiment whether the molecular monolayer is well behaved. The surface tensiometer produced by KINO SCIENTIFIC INSTRUMENT PTE. LTD. shows the surface pressure.

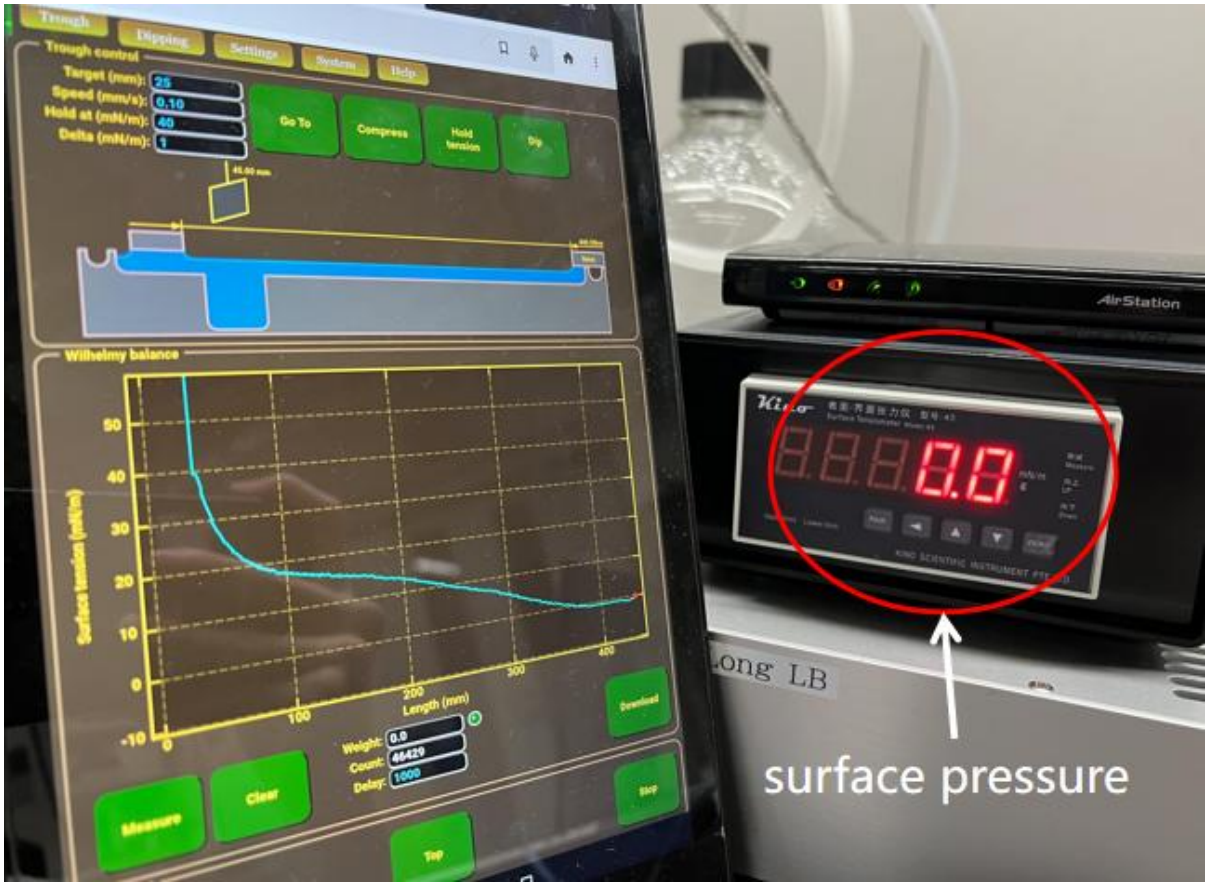

Fig .3.2 Left: LB controller controlling target distance, compression speed, holding pressure, dipping speed, etc. and showing compression distance, dipping distance, and the surface pressure-length curve. (LB controller in this figure is connected to LL 2.) Right: surface tensiometer showing the surface pressure.

The area of the compressed region is obtained by multiplying the distance between barriers (or distance from barrier to end) by the width of the trough. The value is then divided by the number of sample molecules spread on the water surface to get the area occupied by each molecule, which is the molecular area. That is, the calculation formula of the molecular area (A) is:

$$A = \frac{S_A}{N_S} = \frac{W \times L_{Dis}}{C \times V \times N_A} \ ,$$

where: A—molecular area, S_A—area of the compression region, N_S—number of molecules, W—width of the trough, L_{Dis}—distance between the barriers (or distance from the barrier to the end point), C—molecular concentration, V—solution volume, N_A—Avogadro constant (6.02×10^{23}).

The motorized lifter next to the LB trough is used to lift or immerse the solid substrate, as shown in **Fig. 3.3**. Lifting or immersion speed can also be controlled through the above tablet PC.

Fig. 3.3 Motorized lifter, used to lift or immerse solid substrate.

3.3. Preparation of the Langmuir film

3.3.1 Preparation of solutions

For preparing each POSS solution, a 1 mg sample of POSS was added to 5 ml of chloroform. The mixture was shaken in a volumetric flask to ensure thorough mixing of the POSS sample and chloroform until all of the POSS was fully dissolved in the chloroform, forming a homogeneous solution. Agitation of the solution was continued until the solution became uniformly transparent.

3.3.2 Spread and Compression at the air-water interface

At the beginning of the experiment, the subphase needed to be prepared first. For this study, deionized (DI) water (18 MΩ) was used as the subphase, which is a relatively common choice. DI water was obtained from a Direct-Q 5 UV Water Purification System from Merck.

First, the internal surface of the LB trough needed to be cleaned to ensure the purity of the subphase. Acetone is effective for the cleaning purposes. Using a lint-free wipe soaked in acetone, the internal surface of the LB trough was wiped to clean residue or dust. After the acetone rapidly evaporated, DI water was immediately added to the LB trough until the liquid level was in contact with the barriers, so that the barrier can sweep across the surface of the subphase and compress the molecules. For each LB trough, the volumes of water added in LL 1, LL 2, NIMS 1 and NIMS 2

were 150 mL, 400 mL, 250 mL and 1000 mL, respectively.

The Wilhelmy plates used in NIMS 1 and NIMS 2 are filter papers with a size of 1 cm × 1 cm. While the material of the plate used in LL 1 and LL 2 is platinum, and its size is 2.3 cm × 1.2 cm. The reason for choosing a platinum plate instead of a paper filter is that while paper filter is cheaper and easier to replace, it tends to get dirty easily, whereas platinum plates can be flame cleaned and reused. For the platinum plate, before performing surface pressure measurements, it should be cleaned by burning with an alcohol lamp until plate turning into red and then installed on the pressure sensor. To zero the surface pressure reading, as shown in **Fig. 3.4**, the Wilhelmy plate was slowly lowered with a micrometer stage until it contacted the subphase surface while monitoring the surface pressure value displayed on the surface tensiometer display. The ideal surface pressure for DI water is around 72 mN/m. Considering environmental factors and other influences, the actual displayed surface pressure should be within the range of 72 mN/m ± 1 mN/m. Deviation of the measured value from the expected value indicates insufficient cleanliness of the LB trough or the presence of impurities in the subphase. If such a deviation is observed, it is necessary to remove the subphase, clean the LB trough with acetone again, and repeat the above process until the surface pressure displays a reasonable value. The surface pressure reading is then set to zero to prepare for the next experimental steps.

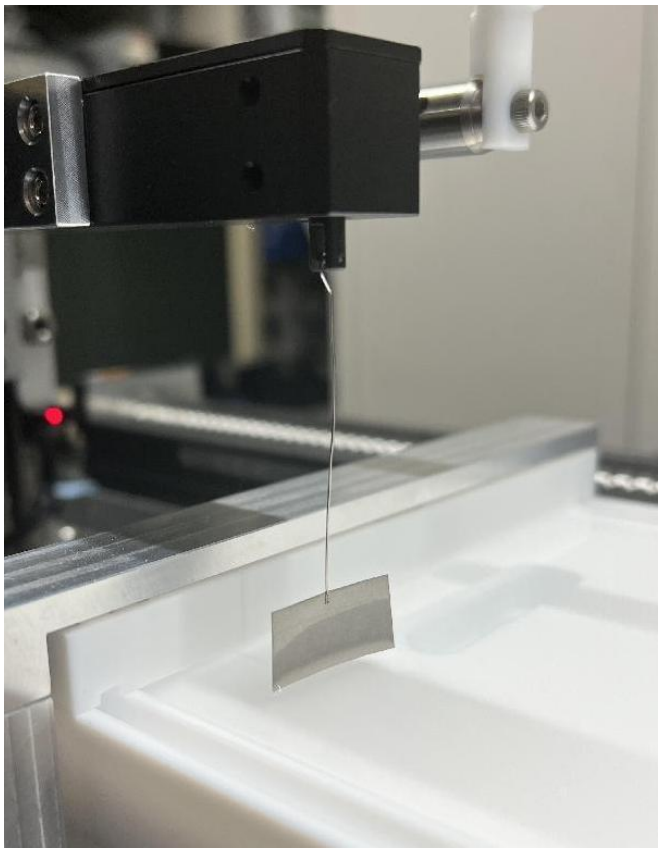

Fig. 3.4 The Wilhelmy plate is installed on the force sensor and lowered slowly until it contacts with the surface of the subphase.

These steps ensure the purity and stability of the subphase, allowing for reliable surface tension measurements. By carefully following these procedures and conducting repeated experiments, accurate data can be obtained.

The specific spread and compression process is as follows. A certain amount of the prepared solution is dropped evenly and slowly onto the air-water interface with a micro-syringe to ensure uniform spread of molecules over the entire surface. The volume of solution taken varies depending on the size of the LB trough, which will be explained in detail in Chapter 4. At this stage, the organic solvent (chloroform) carries the POSS molecules, dispersing them on the water surface. The system is then left undisturbed for 15 min, allowing sufficient time for the solvent molecules to fully evaporate. It is important to note that an excessively long waiting time may result in the aggregation of molecules.

After the solvent has evaporated, the barriers within the LB trough gradually move, applying pressure to the monolayer, and an ordered and stable Langmuir monolayer begins to form. The moving speed of the barrier was usually set at 0.1 mm/s. That is, the compression speed of the LB trough with only one barrier is only half of that of the LB trough with two barriers. The benefit of a slower compression process is to improve the quality of the monolayer, allowing molecules to align and pack more effectively at the air-water interface, reducing the possibility of structural defects, and enhancing the uniformity of the monolayer. Additionally, it helps mitigate potential damage or disruption to the monolayer during the transfer process, thus improving transfer efficiency.

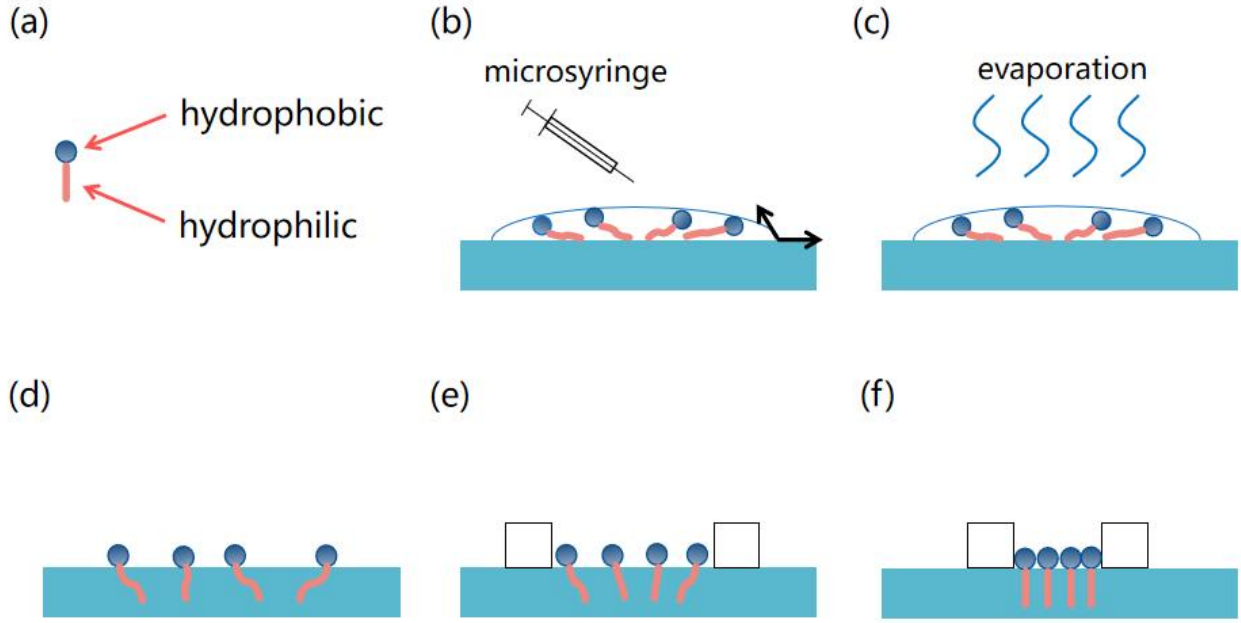

Fig. 3.5 (a) The silica core of the amphiphilic POSS molecule is hydrophobic and faces the air, and the hydrophilic substituents face the water. (b) Use a micro-syringe to drop a certain amount of solution evenly and slowly onto the air-water interface. (c) Wait 15 min for the solvent molecules to evaporate. (d) After the solvent evaporates, the POSS molecules spread on the water surface. (e) Barriers within the LB trough gradually move, applying pressure to the monolayer. (f) An ordered

and stable Langmuir monolayer begins to form.

Throughout the compression process, the changes in the molecular area and surface pressure are recorded. By monitoring and measuring these changes at different stages of compression, the data necessary for constructing the π-A isotherm is obtained.

3.3.3 Transfer to solid substrate

After completing the compression process described in Section 3.3.2, the π-A isotherm of a POSS can be obtained. Due to the repeatability of the π-A isotherm, according to the morphological changes of the monolayer displayed by π-A isotherm under different surface pressures, it can be used as a basis to select the appropriate surface pressure to transfer the film.

A glass substrate was then fixed to a motorized lifter and slowly dipped into the DI water by adjusting the vertical descent using the LB controller. For most experiments, this was done before spreading the POSS molecules on the subphase surface, so that the film transfer could be performed while the glass substrate was slowly lifted out of the water.

During the subsequent compression process, as the barriers continue to compress, the surface pressure continues to increase. Once the surface pressure reaches the predetermined value, the substrate is slowly lifted. At this point, some molecules are gradually transferred to the substrate, reducing the number of molecules at the air-water interface, resulting in a decrease in surface pressure. This phenomenon is particularly pronounced at high surface pressures due to the denser arrangement of molecules.

For this reason, a holding pressure and delta for the system is set, as shown in **Fig. 3.6**. When the pre-set holding pressure is reached, the barriers stop moving and the substrate begins to be lifted. As the substrate is lifted, if the surface pressure drops more than the value of delta below the holding pressure, the barrier automatically starts to slowly compress again until the surface pressure returns to the holding pressure, at which point the barrier stops moving once again. For example, if the holding pressure is set to 40 mN/m, and the delta is set to 1 mN/m, the transfer process begins when the surface pressure reaches 40 mN/m. During the transfer process, if the surface pressure drops below 39 mN/m, the barriers will start moving again until the surface pressure rises back to 40 mN/m. Typically, in a single transfer, the process of maintaining surface pressure is repeated multiple times to ensure effective transfer of the film.

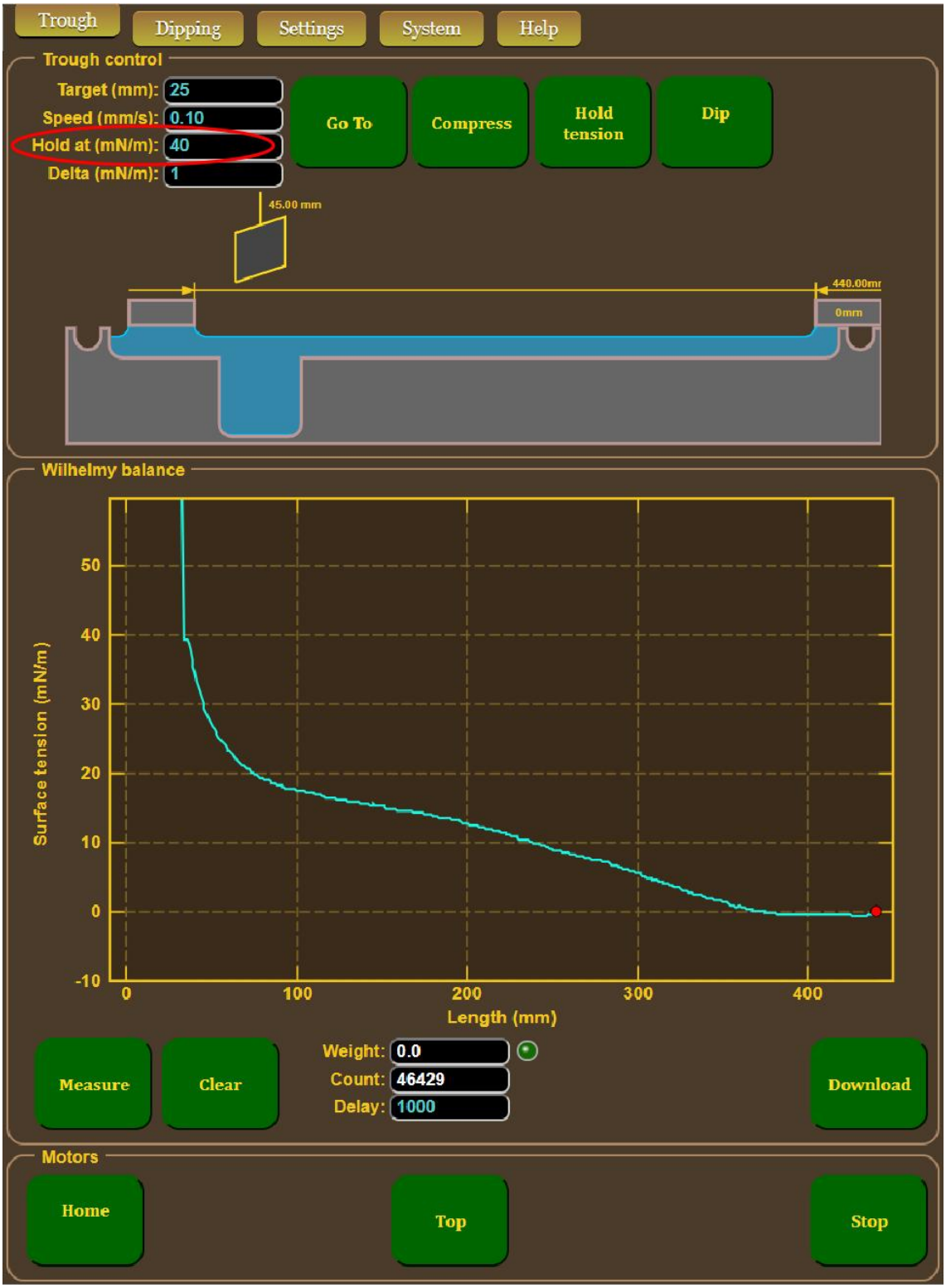

Fig. 3.6 The main control page of the LB system. Inside the red circle is the preset holding pressure.

Throughout the process, the substrate maintains a slow upward movement. The dipping page of the LB controller is shown in **Fig. 3.7**, which can control the lifting and lowering of the lifter. Since there is only one dip count for this experiment, after immersing the substrate in the subphase, there is only a unidirectional lifting process. Therefore, the up speed is a crucial parameter. In order to effectively transfer the monolayer without waiting too long for molecular aggregation, the up speed

is set to 0.1 mm/s.

Fig. 3.7 The dipping page of the LB controller. Inside the red circle is the crucial lifting speed parameter (Up speed).

The surface of the glass substrate is usually hydrophilic, while the silica core of POSS is hydrophobic. The ideal orientation of the transferred POSSs should be as shown in **Fig. 3.8**. However, due to the unique structure of POSS and factors such as hydrogen bonds and intermolecular forces, the orientation of POSSs will not be vertical to the substrate but should be inclined at a certain angle to the substrate.

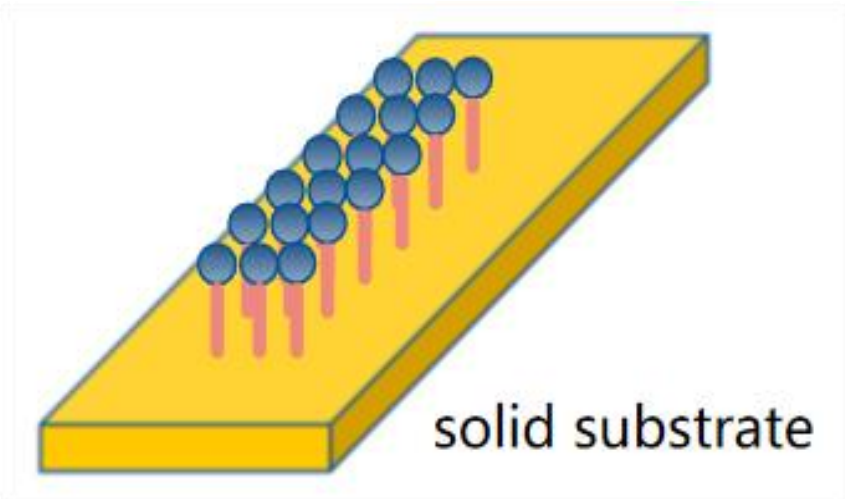

Fig. 3.8 The ideal orientation of the transferred POSSs.

3.4. Atomic force microscopy (AFM) measurement

To observe the thin film surface morphology and surface homogeneity, atomic force microscopy (AFM) measurement was conducted on every sample. The scanning process in AFM involves precisely positioning a probe needle above the sample surface and systematically scanning it over a defined area. As the probe moves across the surface that has height variations, the atomic forces between the tip and the sample will change. The force is measured by observing the deflection of a soft cantilever made of Si or Si_3N_4. The deflection is measured with a position-sensitive detector (PSD) by observing the shift of a laser beam reflected from the back of the cantilever, as shown in **Fig. 3.9**.

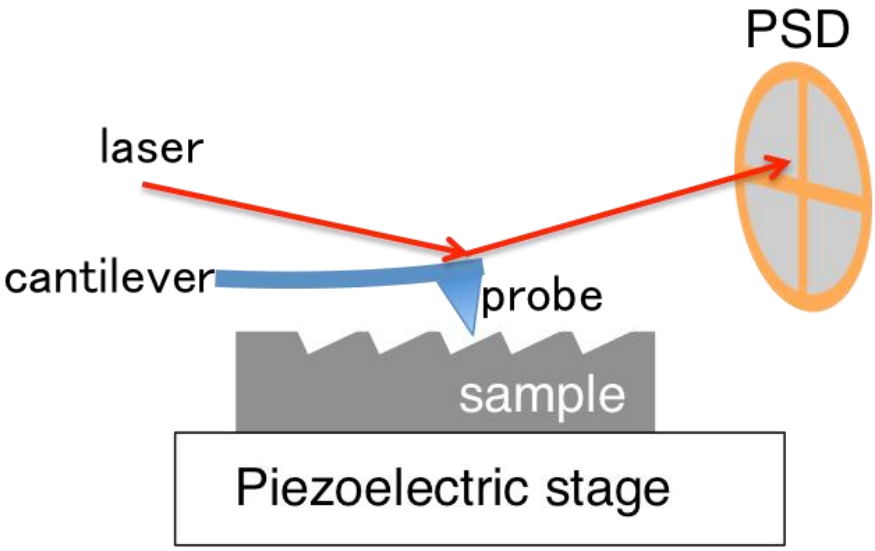

Fig. 3.9 Schematic illustration of optical-lever system employed in AFM for detecting the displacement of the probe.

In this study, the Shimadzu SPM-9600 AFM was used to measure the surface morphology, as shown **in Fig. 3.10**. In AFM measurement, a vibration isolation system (TS-150, Table Stable Ltd.) was placed under the AFM, and used to reduce external mechanical vibrations. All measurements were done in the lateral force (LFM) contact mode. In contact-mode measurement, a piezoelectric stage under the sample is used to adjust the sample height so that the tip cantilever deflection is close to a pre-determined set-point value, which corresponds to a chosen contact force. The output signal of the piezo stage control voltage is then presented as a 2D mapping AFM image after the tip has scanned over a certain area on the surface [45].

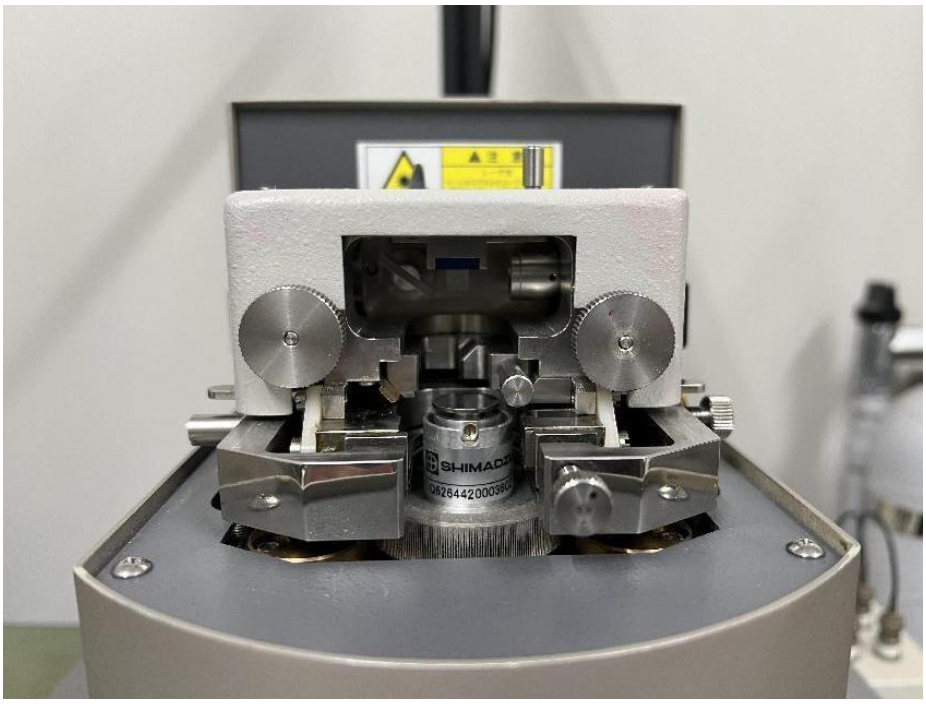

Fig. 3.10 The AFM equipment used in this study, Shimadzu SPM-9600 AFM.

Chapter 4

Results and Discussion

4.1. Comparison of LB equipment

Initially, an analysis of the performance of our lab-developed LB system was conducted. To facilitate a comprehensive comparison with commercial LB systems at NIMS, the initial choice was made to adopt a similar approach by employing two barriers. This setup allowed for a direct assessment of the disparities between our LB system and the commercial LB systems. Different quantities of molecules were introduced into the systems based on the diverse sizes of LB troughs. The initial molecular area where the surface pressure starts to increase in each LB trough is shown in **Table. 5**. Four POSSs belonging to the first category and one amphiphilic POSS belonging to the second category were selected. Due to the time required for ordering and delivery, there were only these five POSSs in the lab at that time.

Table. 5 The initial molecular area in each LB trough. (nm^2/molecule)

	Name	LL 1	NIMS 1	NIMS 2
POSS-1	PSS-Octamethyl substituted	0.89	0.99	2.43
POSS-2	PSS-Octaphenyl substituted	1.72	1.91	2.80
POSS-3	PSS-Octacyclohexyl substituted	1.80	1.91	2.93
POSS-4	PSS-Octakis(dimethylsilyloxy) substituted	1.69	1.88	2.76
POSS-5	PSS-[3-(2-aminoethyl)amino]propyl-heptaisobutyl substituted	1.53	1.70	2.49

By compressing five POSSs, their π-A isotherms on three double-barrier LB systems were obtained, as shown in **Fig. 4.1**. The barriers all move at the same speed, fixed at 0.1 mm/s. But because the widths of the troughs are different, the area speeds are also different: LL 1——8 mm^2/s, NIMS 1——10 mm^2/s, NIMS 2——15 mm^2/s. Changing the area speed has some effect on the aggregation behavior and may result in slight differences in the molecular area (horizontal axis) of

the final π-A isotherm, but does not affect the surface pressure (vertical axis) at each stage of monolayer formation process.

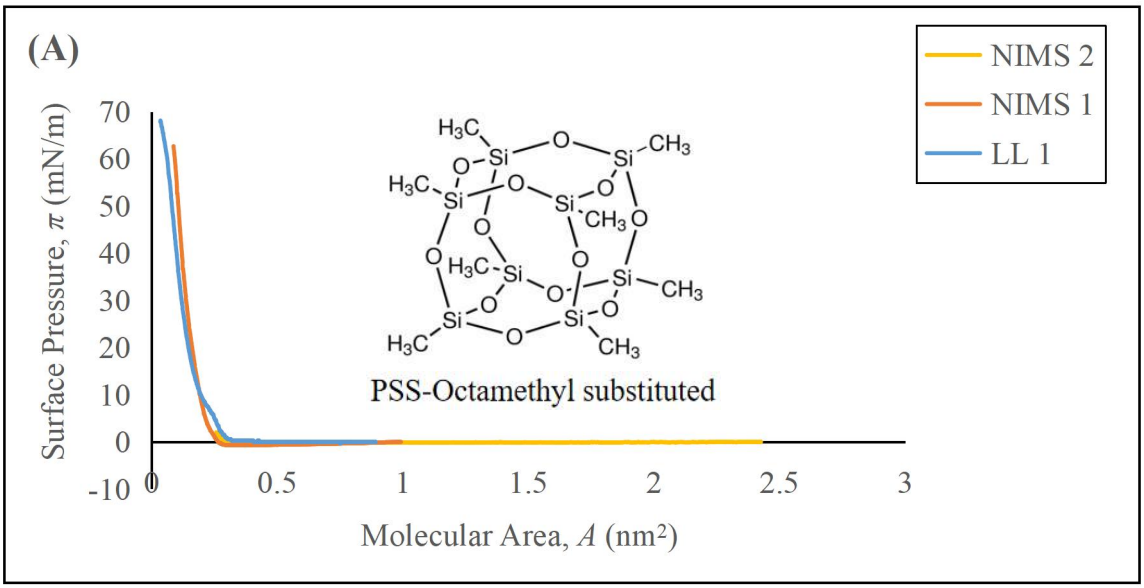

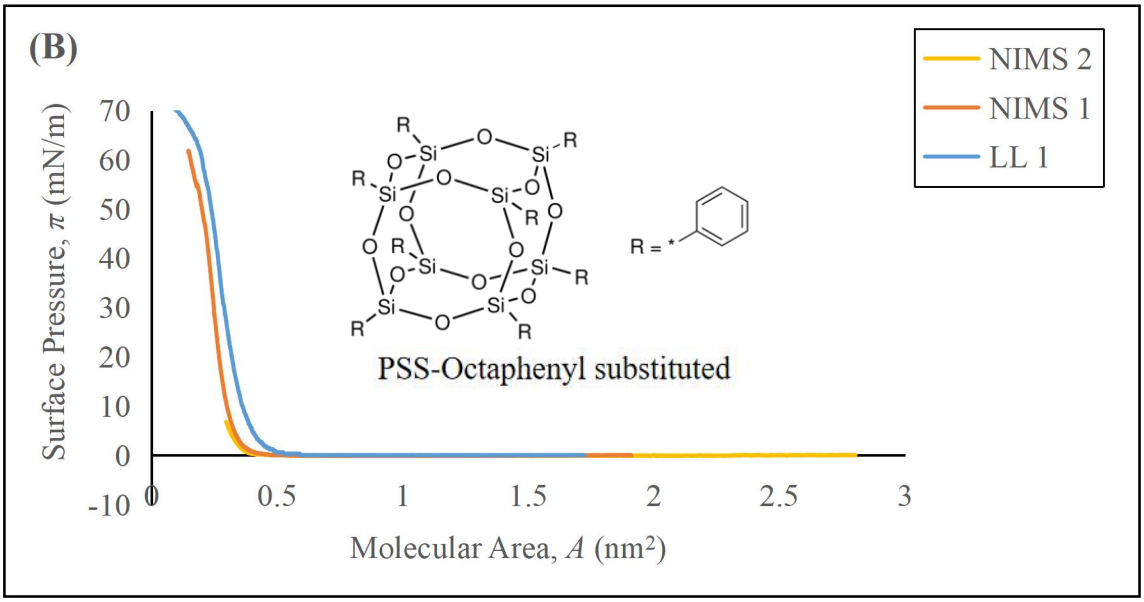

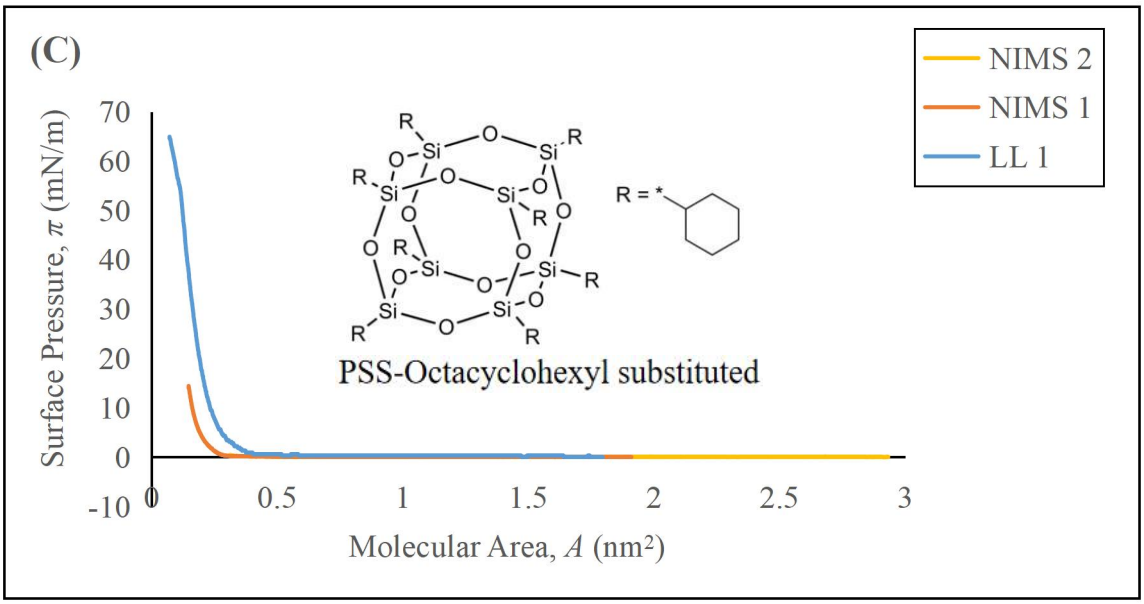

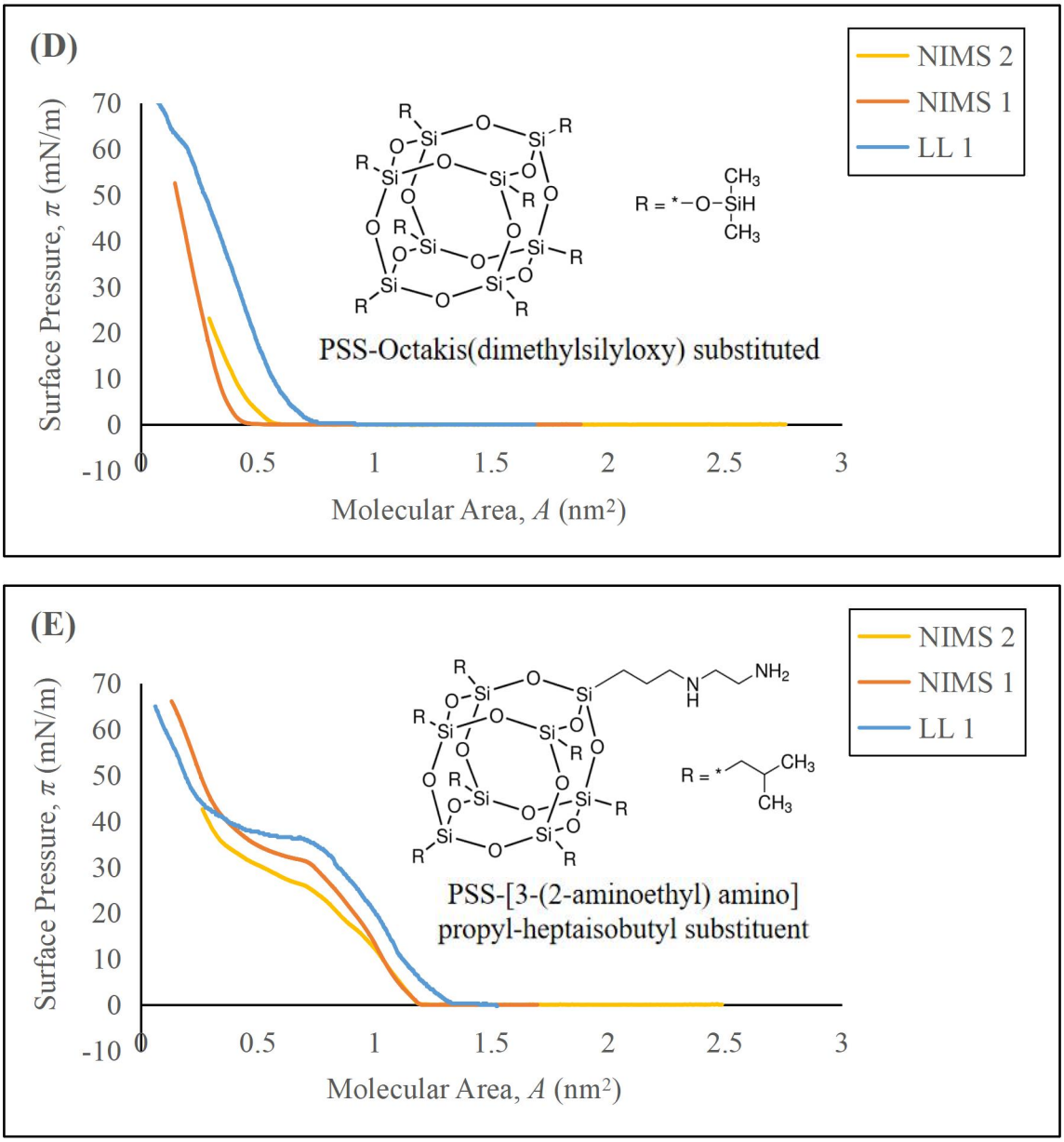

Fig. 4.1 Schematic diagram of *π-A* isotherms obtained by compressing five different POSSs on the double-barrier LB system of Lippmaa Lab (blue line: LL 1, 250 mm × 80 mm) and two double-barrier LB systems of NIMS (orange line: NIMS 1, 334 mm × 100 mm; yellow line: NIMS 2, 544 mm × 150 mm) respectively.

The ideal *π-A* isotherm is independent of the size of the LB trough, solution concentration, or spreading volume. But in practical situations, variations can occur due to factors such as intermolecular interactions and intermolecular forces. However, for the first category, which refers to the first four POSSs (POSS-1 to 4), there are significant differences in the *π-A* isotherms observed after compressing them through three different LB troughs, and the transitional state cannot be determined in the *π-A* isotherm. Their behavior is influenced by the available space for spreading at the air-water interface. It indicates that their molecular arrangement extends beyond a single layer and involves stacking or aggregation of molecules in the vertical direction. It can be

speculated that the first category of POSSs tend to form 3D aggregations at the interface rather than forming 2D monolayers. The reason behind this is that these four types of POSS lack hydrophilic functional groups, and as a result, the intermolecular interactions between the POSS molecules become dominant, leading to the formation of random 3D structures. It also implies that the first category of POSSs cannot serve as reasonable samples to validate the feasibility of the LB system in our lab. The similar isotherms exhibited by LL1 and NIMS1 in **Fig. 4.1 (A)** and **(B)** are merely coincidental.

The *π-A* isotherm of POSS-5 with amino groups is valuable for comparing our lab's LB system with commercial LB system, as it is amphiphilic and exhibits a distinct transition state, tending to form 2D monolayers. As shown in **Fig. 4.1(E)**, there are slight differences in the *π-A* isotherms of POSS-5 in the three LB troughs, which are caused by different compression speeds. The barrier movement speed in all LB systems was set at 0.1 mm/s, but due to the different widths of the troughs, the compression speeds were not the same, resulting in varying interaction times of the molecules at the interface. This is the reason why the three *π-A* isotherms are not identical, although they all exhibit similar shapes. **Fig. 4.1 (E)** demonstrates the reproducibility of the *π-A* isotherm, and also proves the feasibility of the LB system fabricated in our lab.

POSSs are not typical amphiphilic molecules, in order to achieve a monolayer, a larger-sized LB trough is preferable, as it provides more space for the molecules to arrange freely and facilitates the transfer of a larger area of the monolayer onto a solid substrate. Additionally, a larger trough provides a more stable and reliable measurement platform, thereby reducing experimental errors and improving the accuracy of the *π-A* isotherms.

Considering the above reasons, another LB trough was constructed as shown in **Fig. 4.2**. By using a larger-sized trough compared to LL 1 and only setting up one barrier, it allows for a smaller compression speed. And it is beneficial for transferring larger and more layers LB films.

During the transfer process, the groove where the substrate is placed is set at the opposite end of the initial position of the barrier, which does not affect the transfer efficiency.

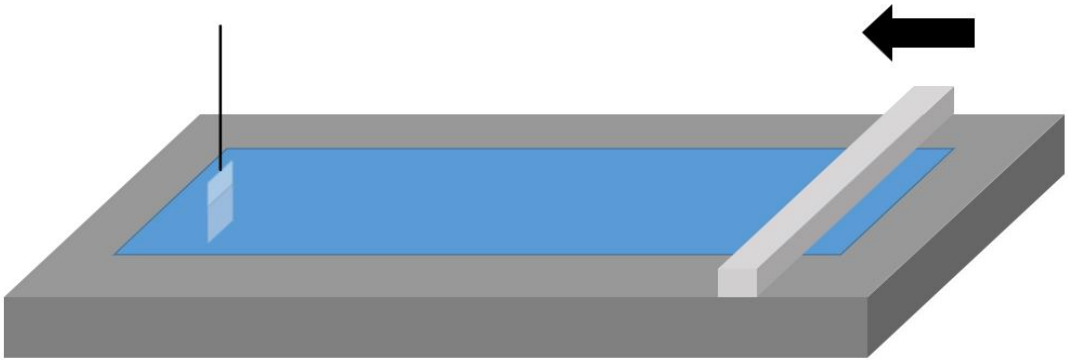

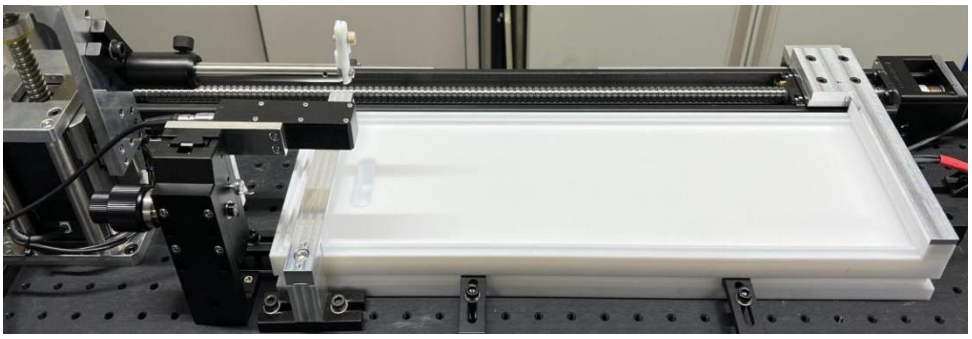

Fig. 4.2 Top: Schematic illustration of the improved LB equipment.
Bottom: Photo of the improved LB of LL 2 equipment.

One of the second category of POSSs with amphiphilicity was selected to evaluate the LB of LL 2 system. Compression was performed at two different compression speeds, and the corresponding π-A isotherms were obtained, as shown in **Fig. 4.3**. The same volume and configuration of solution were used, meaning an equal number of molecules at the interface, to ensure that all variables except compression speed remained consistent.

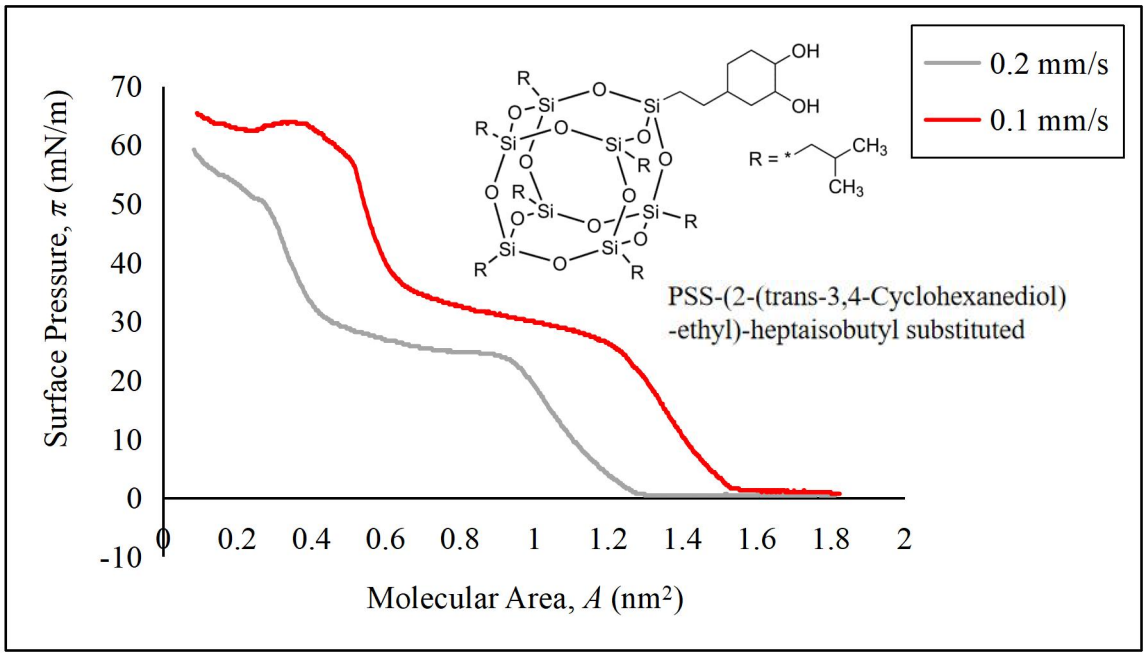

Fig. 4.3 The corresponding π-A isotherms were obtained by compressing the POSS-6 through the LB system of LL 2 at compression speeds of 0.2 mm/s (gray line) and 0.1 mm/s (red line), respectively. Except for compression speed, all other variables were held constant.

By comparing the two curves, it can be observed that the initial plateau surface pressure remains around 25 mN/m, and the molecular area of the red line increases by about 0.3 nm^2 compared with that of the gray line from when the surface pressure starts to rise until the compression ends. And because the molecular area corresponding to each stage increases, the red line as slower compression speed provides further information of the π-A isotherm at the end of compression. In other words, the slower compression speed allows more time for molecular rearrangement and

adsorption, so that the A_0 of the π-A isotherm tends to the region with a larger molecular area. The surface pressure changes at the transition state are nearly identical for both curves, indicating a similar internal transition process in the monolayer.

In summary, it can be seen from **Fig. 4.2 (E)** that the π-A isotherms of POSS with amino groups in each LB trough are almost the same, indicating that the performance of our lab's LB trough is comparable to that of the commercial LB trough used by NIMS. Meanwhile, **Fig. 4.3** illustrates the feasibility of the improved LB system, and the lower compression rate achieved through it benefits obtaining more complete molecular layer changes. The subsequent compression and transfer processes were performed using the improved LB system mentioned above, and the compression speed was always set at 0.1 mm/s.

4.2. π-A isotherms of POSS

The π-A isotherms of each type of POSS were obtained using the LB system, and they are discussed by category.

As the surface pressure increases from zero, the molecular layer undergoes structural changes due to intermolecular interactions. The molecular area at which the surface pressure begins to increase, which is A_0, can be determined from the π-A isotherm. In order to analyze the behavior and state of the molecules at the interface, it is necessary to know the molecular diameter of each type of POSS. By estimating the molecular cross-sectional area from this value and comparing it with the A_0 value, information such as the packing modes of different POSS molecules at the interface can be inferred. In this study, Chem3D software, a tool for chemical molecule modeling and visualization, was employed to obtain the molecular diameter. Each POSS molecule was modeled according to its molecular structure, and the molecular diameter was obtained by measuring the distance between the two farthest atoms within the molecule. It should be noted that the Si-O cage structure of POSS is stable and difficult to deform, but the substituents are flexible and can easy change their orientation. Therefore, in addition to the distance between the furthest atoms, the diameter of the Si-O cage also needs to be considered.

The sizes of the cubic silica cores of nine POSSs were first measured using Chem3D, as shown in **Fig. 4.4**. In ideal models, the core structures of different POSSs are the same, so their dimensions should be the same. However, the external groups will affect the core to achieve energy minimization. Therefore, there may be slight variations in the core size, but the difference is so small that it can almost be ignored. The molecular diameter is only an approximate method to describe the molecular size, and more precise parameters for a specific molecule may require further theoretical research in combination with other techniques. The distances between diagonal Si and diagonal C were measured in the crystal structure of POSS-1 [46] by Mercury software, in order to verify whether the molecular diameters estimated by Chem3D are accurate. The obtained

results are shown in **Fig. 4.5**, which are 0.56 nm and 0.91 nm, respectively, which match the estimated values of 0.57 nm and 0.95 nm, obtained by Chem3D as shown in **Fig. 4.4(A)** and **Fig. 4.6(b)**.

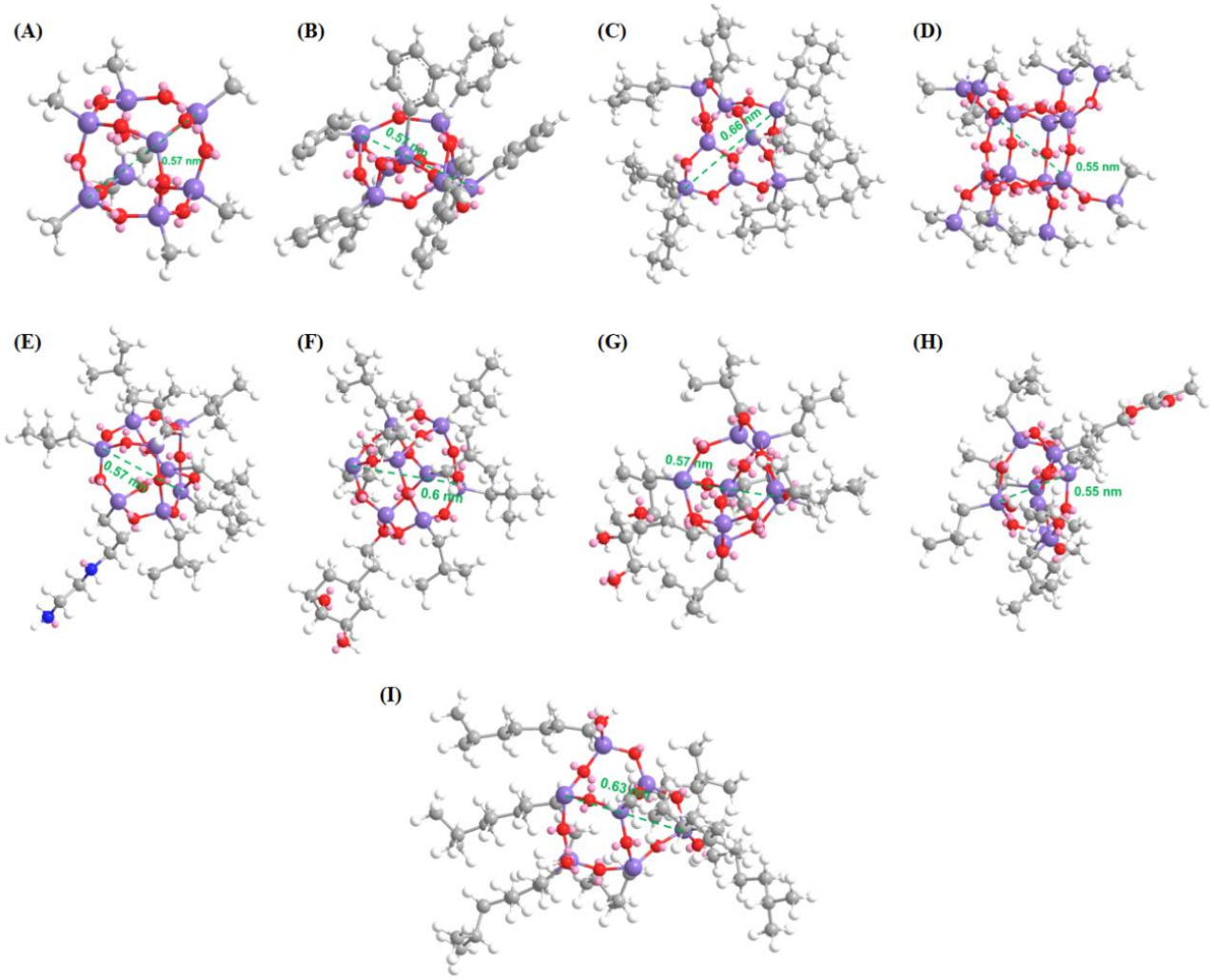

Fig .4.4 For the nine POSSs obtained through Chem3D modeling, (A) POSS-1, (B) POSS-2, (C) POSS-3, (D) POSS-4, (E) POSS-5, (F) POSS-6, (G)POSS-7, (H) POSS-8, (I) POSS-9. The distance between two diagonal silicon atoms are marked in each core.

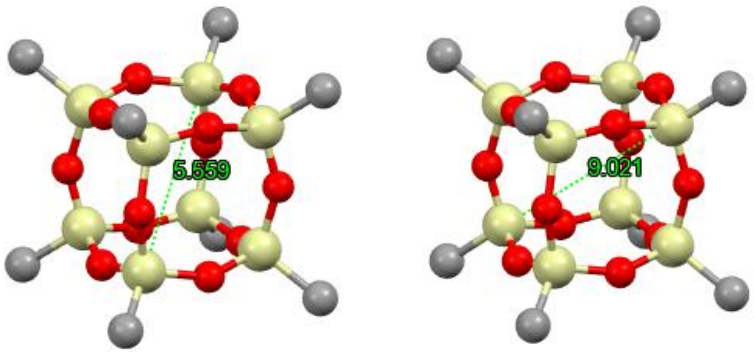

Fig. 4.5 The distances between diagonal Si and diagonal C of the crystal structure of POSS-1 measured by Mercury.

Based on the measurement of the distance between two diagonal silicon atoms inside the core, the diameter of the cage core of all POSS types was determined to be about 0.6 nm. Due to the strong stability of the core structure, this sets the lower diameter limit that POSS molecules can achieve, called the core diameter.

Fig. 4.6 shows the *π-A* isotherms of the four POSS molecules belonging to the first category, along with their molecular structures and diameters obtained through Chem3D modeling. The diameters measured at this time are the maximum diameters that POSS molecules can achieve without being affected by external effects.

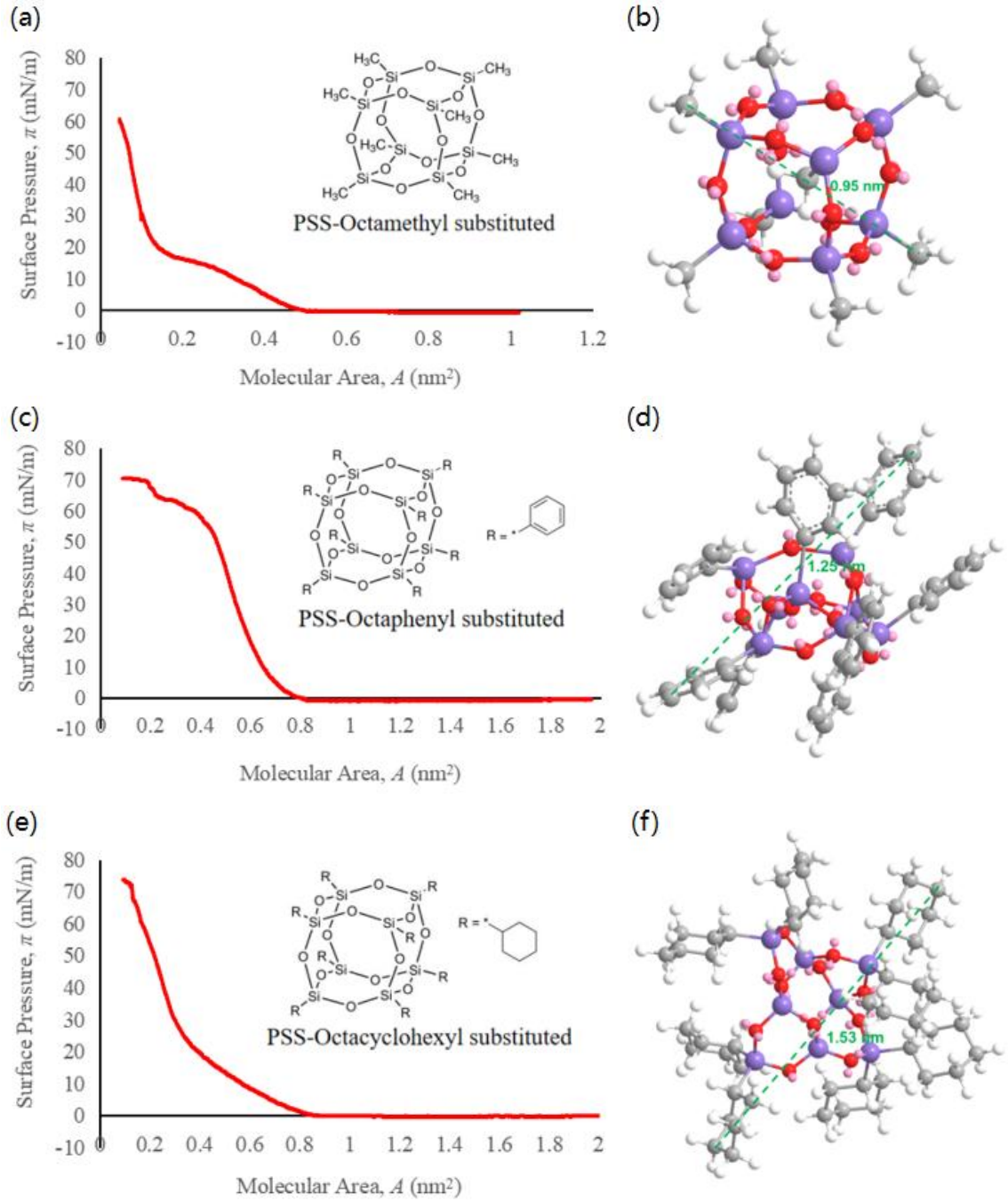

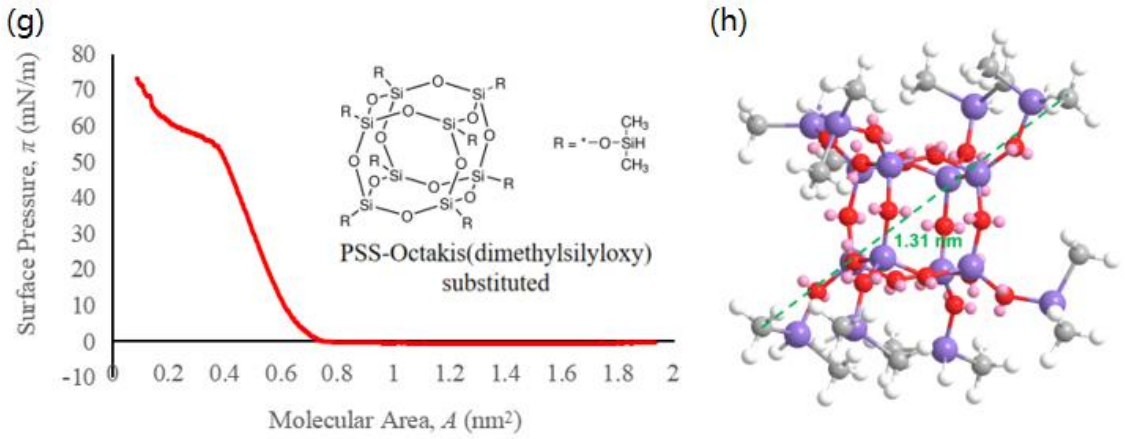

Fig .4.6 Belonging to the first category of POSS, the *π-A* isotherms and the molecular structure and diameters obtained by Chem3D modeling of (a-b) POSS-1, (c-d) POSS-2, (e-f) POSS-3, (g-h) POSS-4.

The POSS molecule can be approximated as a spherical structure. According to the molecular diameters measured in **Fig. 4.4** and **Fig. 4.6**, the core cross-sectional area and maximum cross-sectional area of a single molecule, that is, the occupied area, are calculated, as shown in **Table .6**.

Table .6 The minimum and maximum cross-sectional areas of the first category of POSSs.

Name	Core diameter (nm)	Maximum diameter (nm)	Core cross-sectional area (nm^2)	Maximum cross-sectional area (nm^2)	A_0 (nm^2)
POSS-1	0.57	0.95	0.26	0.71	0.48
POSS-2	0.57	1.25	0.26	1.23	0.82
POSS-3	0.57	1.53	0.26	1.84	0.86
POSS-4	0.57	1.31	0.26	1.35	0.78

Since the eight substituents of the first category of POSS are all the same, they are completely symmetrical and have a high degree of freedom in molecular orientation. Considering all these four POSS molecules, it is evident that their A_0 values are significantly smaller than their maximum cross-sectional area, with differences ranging from 0.3 to 1. For POSS-3 and POSS-4, their A_0 values are just half of the maximum cross-sectional areas. Since these molecules lack hydrophilic substituents or polar groups, the intermolecular interactions are primarily governed by weak van der

Waals forces. These forces are relatively weak compared to ionic or hydrogen bonding. Weak intermolecular forces cause molecules to form irregular 3D random structures. It can be considered that for POSS without hydrophilic substituents, the molecules tend to form 3D aggregate instead of a uniform monolayer.

The π-A isotherms of the four POSSs of the second category and their molecular structures and diameters, are shown in **Fig. 4.7**. Compared to the first category of POSSs, the second category of POSSs demonstrates significantly superior performance in terms of layer formation in the π-A isotherms.

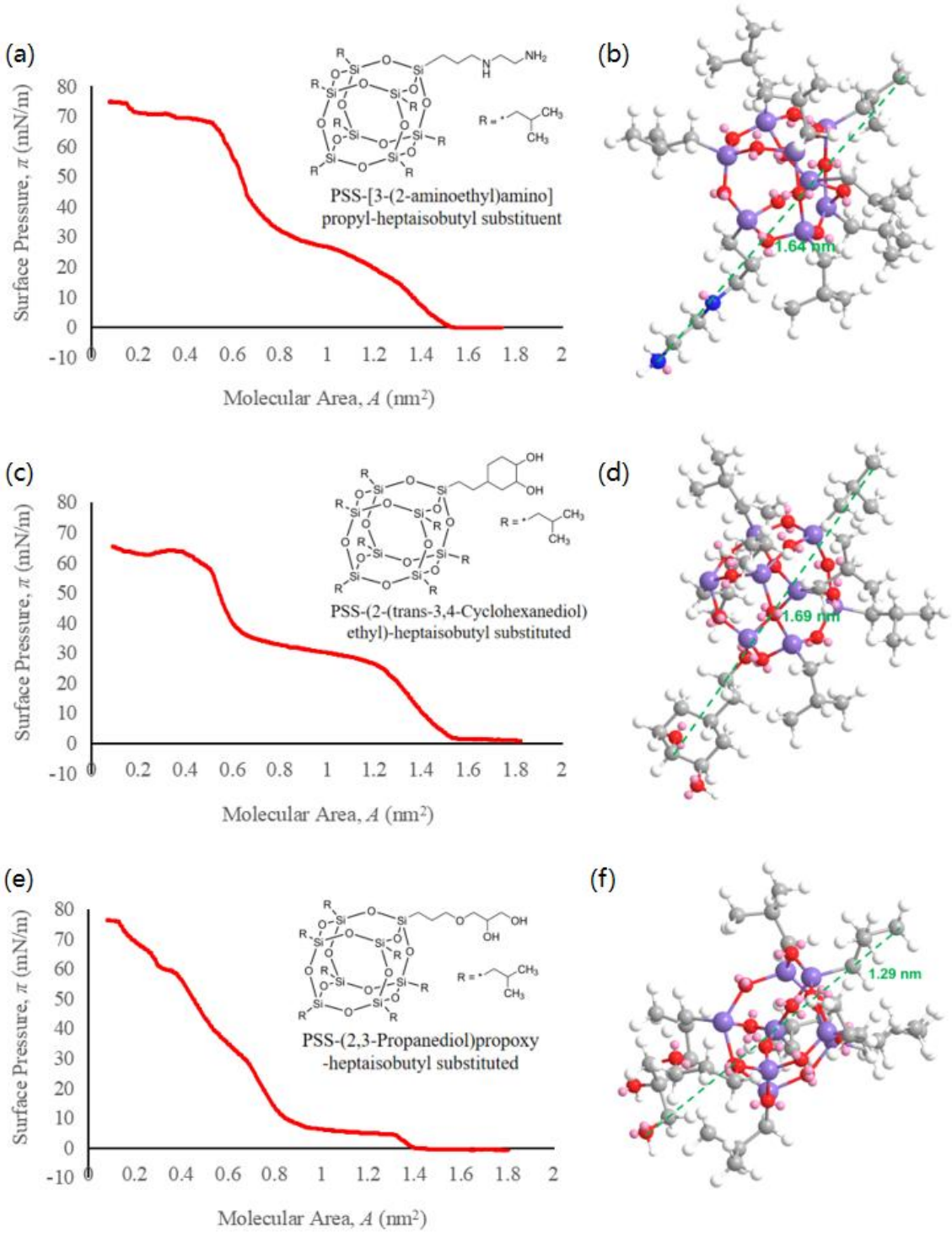

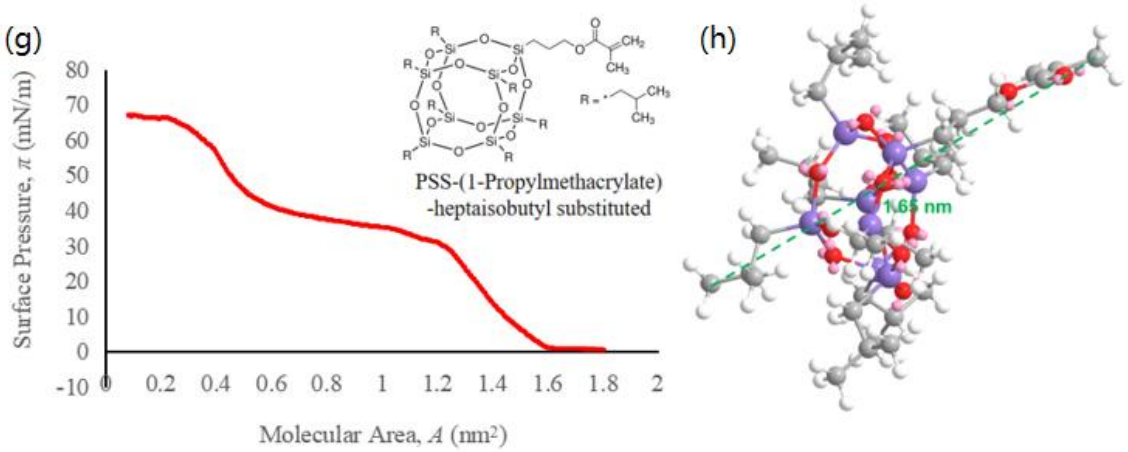

Fig .4.7 Belonging to the second category of POSS, the π-A isotherms and the molecular structure and diameters obtained by Chem3D modeling of (a-b) POSS-5, (c-d) POSS-6, (e-f) POSS-7, (g-h) POSS-8.

Similarly, according to the molecular diameter measured in **Fig. 4.4**, the minimum cross-sectional area of a single molecule is estimated. Considering that for the second category of POSSs, the long chains of their hydrophilic substituents point downwards and are immersed in water, it will not have a great impact on the area occupied by the molecule at the interface. Therefore, when calculating the maximum cross-sectional area, the single hydrophilic substituent is ignored, and the distance from the center point of the core to the farthest C atom in the isobutyl group is calculated as the radius, as shown in **Table .7**. Since the structure of the cage core is very stable, and except for one hydrophilic substituent, the remaining seven substituents of these four POSSs are all isobutyl, so their minimum and maximum cross-sectional areas are almost the same.

Table. 7 The minimum and maximum cross-sectional areas of the second category of POSSs.

Name	Core diameter (nm)	Maximum diameter (nm)	Core cross-sectional area (nm^2)	Maximum cross-sectional area (nm^2)	A_0 (nm^2)
POSS-5	0.57	1.43	0.26	1.61	1.53
POSS-6	0.57	1.46	0.26	1.67	1.57
POSS-7	0.57	1.43	0.26	1.61	1.39
POSS-8	0.57	1.41	0.26	1.57	1.59

By analyzing the A_0 values of the four POSSs and their respective molecular diameters, it was

found that the maximum cross-sectional area is similar to the A_0 value. Except for POSS-7, the difference between the A_0 values and the maximum cross-sectional areas of the other three POSSs are less than 0.1, and A_0 is approximately equal to the area of a single molecule. The A_0 value of POSS-7 is about 0.2 smaller than its maximum cross-sectional area, because the hydrophilic substituent in its long chain contains propanediol, which imparts greater flexibility to the molecule compared to other POSSs.

From a microscopic point of view, as the molecules are compressed and gradually move closer together, the intermolecular spacing gradually decreases. Ideally, when the distance between molecules is reduced to exactly zero, each molecule occupies an area equivalent to its own size. At this critical point, the molecular area reaches an A_0 value of 1.5-1.6, signifying the transition of individual molecules on the interface into a collective entity where they come into contact and the formation of a monolayer commences. Considering that the second category of POSSs have a long chain of hydrophilic substituent, this hydrophilic group enhances intermolecular interactions, promoting changes in molecular orientation, and significantly enhancing the order within the monolayer. Subsequent compression leads to a more compact arrangement of molecules at the interface, while the surface pressure starts to rise, gradually forming a larger area of 2D assembly.

The plateau observed in the π-A isotherm generally indicates a reorganization or transformation of the molecular structure. For these four POSSs, at least two plateaus, representing transition states, have been observed. In such cases, the first-order phase transition corresponds to the rearrangement of molecules at the interface to form a more stable structure. Different side chain characteristics can affect the interaction of molecules at the interface, thereby affecting the surface pressure during the first-order phase transition. 3D aggregation may occur when the surface pressure is gradually increased to reach the first-order phase transition. To specifically analyze the state of the monolayer during this process, it is necessary to conduct AFM measurements of the thin film height of Langmuir monolayers transferred at different surface pressures, and it will be discussed in the next section.

The compression modulus C_s^{-1} values of the second category of POSSs were examined, expressed as a function of surface pressure, as shown in **Fig. 4.8**. According to **Fig. 4.8**, for POSS-5 to 8, the surface pressures of the first troughs that appear from 0 are about 25 mN/m, 30 mN/m, 5 mN/m, and 35 mN/m, respectively, corresponding to the first-order phase transitions in their π-A isotherms. The first peak represents the formation of a monolayer. After the first-order phase transition occurs, according to the intermolecular interactions of the respective POSS molecules, a somewhat ordered 3D structure may be formed on top of the ordered monolayer. Since the purpose of this study is to investigate the 2D assembly of POSSs, the process before the first-order phase transition is mainly considered.

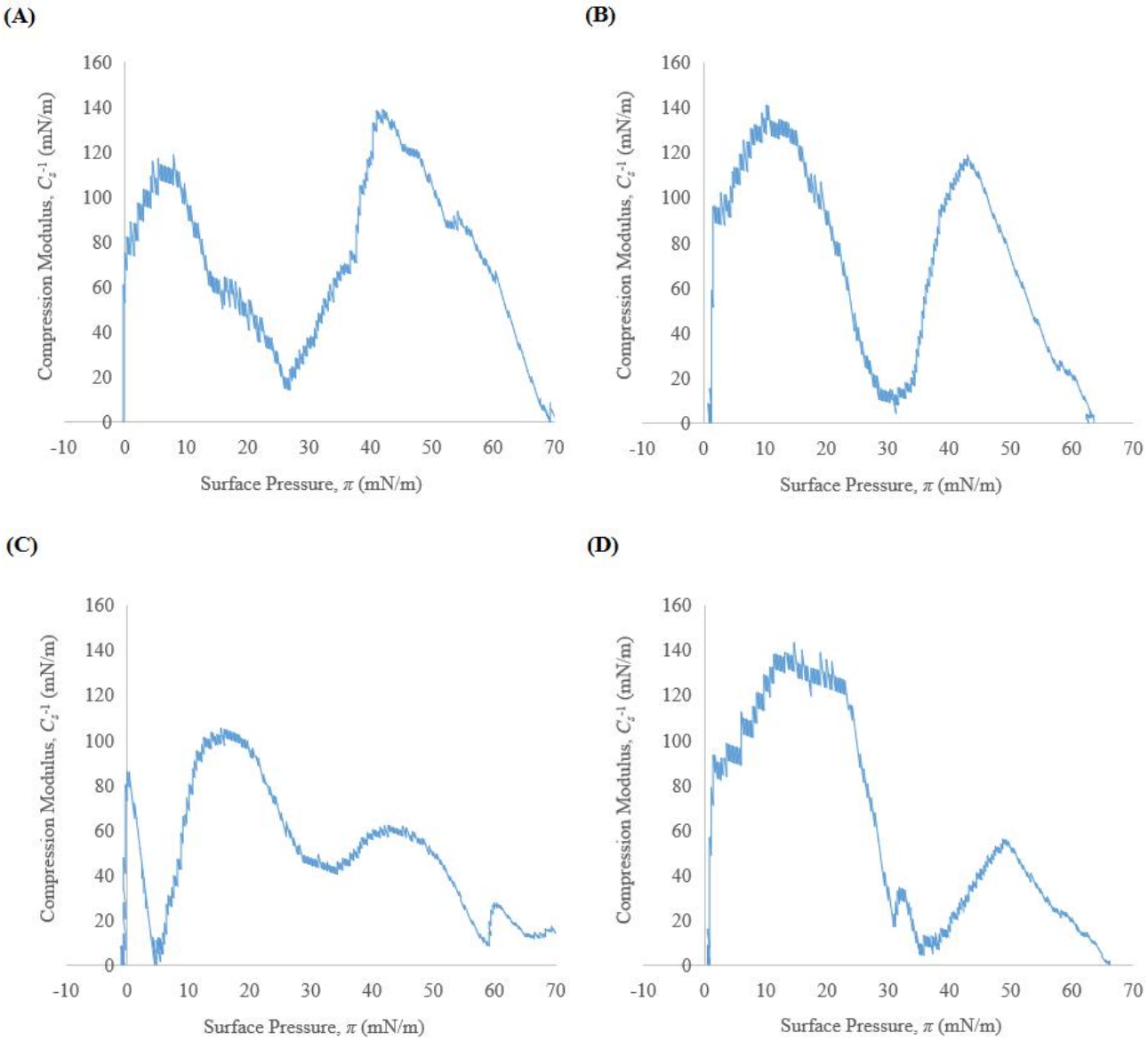

Fig. 4.8 (A), (B), (C), and (D) are the compression modulus C_s^{-1} of POSS-5, POSS-6, POSS-7, and POSS-8, respectively, as a function of surface pressure π.

For POSS-5 to 8, the first peaks of their compression modulus C_s^{-1} are around 80-140 mN/m, indicating that at this time, the state of the monolayers are liquid condensed phase. Among them, the compression modulus Cs^{-1} of POSS-7 is relatively lower, less than 100 mN/m, as shown in **Fig. 4.8 (C)**. This difference may be attributed to the unique properties of its side chains. The presence of propanediol enables POSS-7 molecules to adapt more flexibly to the interfacial environment and interact with surrounding water molecules, leading to lower energy requirements and correspondingly lower compression modulus and surface pressure during the first-order phase transition. In contrast, the side chain characteristics of POSS-5, POSS-6 and POSS-8 may result in a more compact molecular arrangement at the interface, with stronger intermolecular interactions, requiring higher energy and resulting in higher compression modulus and surface pressure during the first-order phase transition.

The last, π-A isotherm, molecular structure, and diameter of the third category of POSS are shown in **Fig. 4.9**.

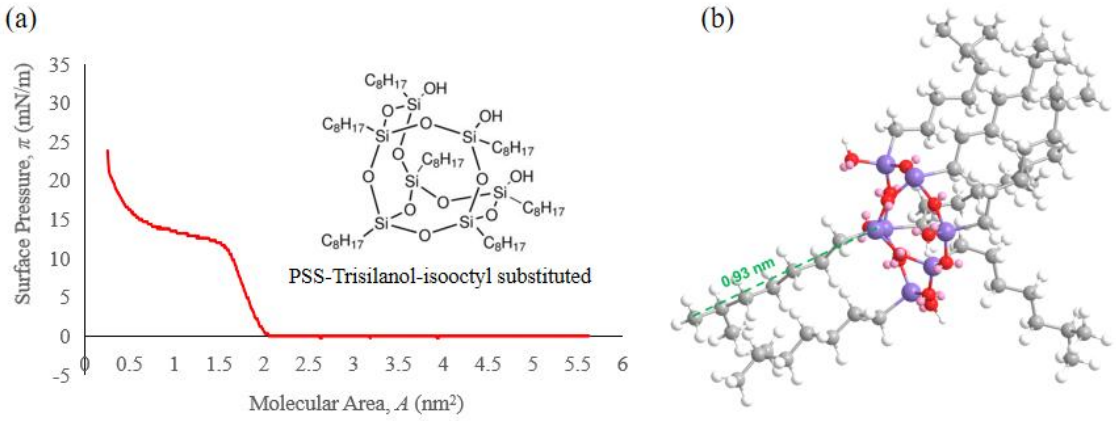

Fig. 4.9 Belonging to the third category of POSS, the π-A isotherm and the molecular structure and diameter obtained by Chem3D modeling of POSS-9.

The third category of POSS is formed by partial hydrolysis of a completely condensed POSS (CC-POSS) analogue, called incompletely condensed POSS (IC-POSS). The POSS-9 used in this study, in which one corner of a CC-POSS is hydrolyzed, is a typical IC-POSS. Compared to the first and second categories of POSSs, the third category has larger substituents on each core silicon atom, resulting in a significantly larger overall molecular size and relative molecular mass.

Due to the special structure of this POSS, it can only be approximated to have a complete cage core like other POSSs and its molecular diameter can be estimated, as shown in **Table. 8**.

Table. 8 The minimum and maximum cross-sectional areas of the third category of POSSs.

Name	Core diameter (nm)	Maximum diameter (nm)	Core cross-sectional area (nm^2)	Maximum cross-sectional area (nm^2)	A_0 (nm^2)
POSS-9	0.63	2.49	0.31	4.87	2.05

From the π-A isotherm, it can be observed that this particular POSS, both in terms of initial molecular area and A_0, is much larger than the first and second categories of POSSs mentioned previously. This can be attributed to its significantly larger molecular diameter. Estimates of its cross-sectional area range widely, making it difficult to define. Furthermore, it also exhibits a first-order phase transition, but the surface pressure during the transition and at the end of compression is lower compared to the π-A isotherms of other POSS categories shown previously.

There are two possibilities for this phenomenon. The first is that the hydrolyzed part of the core exhibits hydrophilicity, making the whole amphiphilic. A second possibility is that POSS-9 forms dimers that spontaneously self-assemble into nonequilibrium crystal structures upon further compression [47]. But this transient state is difficult to capture, and using detectors with faster data acquisition capabilities may be able to decipher this kinetically driven phase transition [47].

Finally, the POSSs are summarized by category. For the first category of POSSs, their A_0 values are much smaller than the largest cross-sectional area, indicating that the weak intermolecular forces and the absence of hydrophilic substituents lead to molecular packing, forming random 3D aggregates. For the second category of POSSs, their A_0 values are nearly the same as the maximum cross-sectional area, indicating that hydrophilic groups greatly enhance the order within the monolayer, resulting in 2D assembly through molecular interactions. And the π-A isotherms all present a transition state, corresponding to the rearrangement of molecules at the interface to form a more stable structure. As for the third category of POSS, its cross-sectional area estimation has a wide range, making it difficult to compare with the A_0 value. Furthermore, although it exhibits a lower surface pressure in the π-A isotherm, it also shows a transition state, possibly implying the formation of dimers.

4.3 Post-transfer AFM image analysis

To investigate the behavior of POSS on glass substrate, several types of POSSs were transferred at different surface pressures according to their respective π-A isotherms. AFM measurements were performed on these samples, and AFM images of their surfaces were obtained.

In Section 4.2, the analysis was performed on the first category of POSSs with hydrophobic substituents, and no significant plateau was observed in their π-A isotherms. The molecules exhibited 3D aggregation at the interface. Therefore, only POSS-1 was chosen for transfer at a surface pressure of 40 mN/m, and subsequent AFM measurements were performed to explore its surface morphology, as shown in **Fig. 4.10**. For reference, AFM measurement was also performed on the pure glass substrate without any POSS transfer.

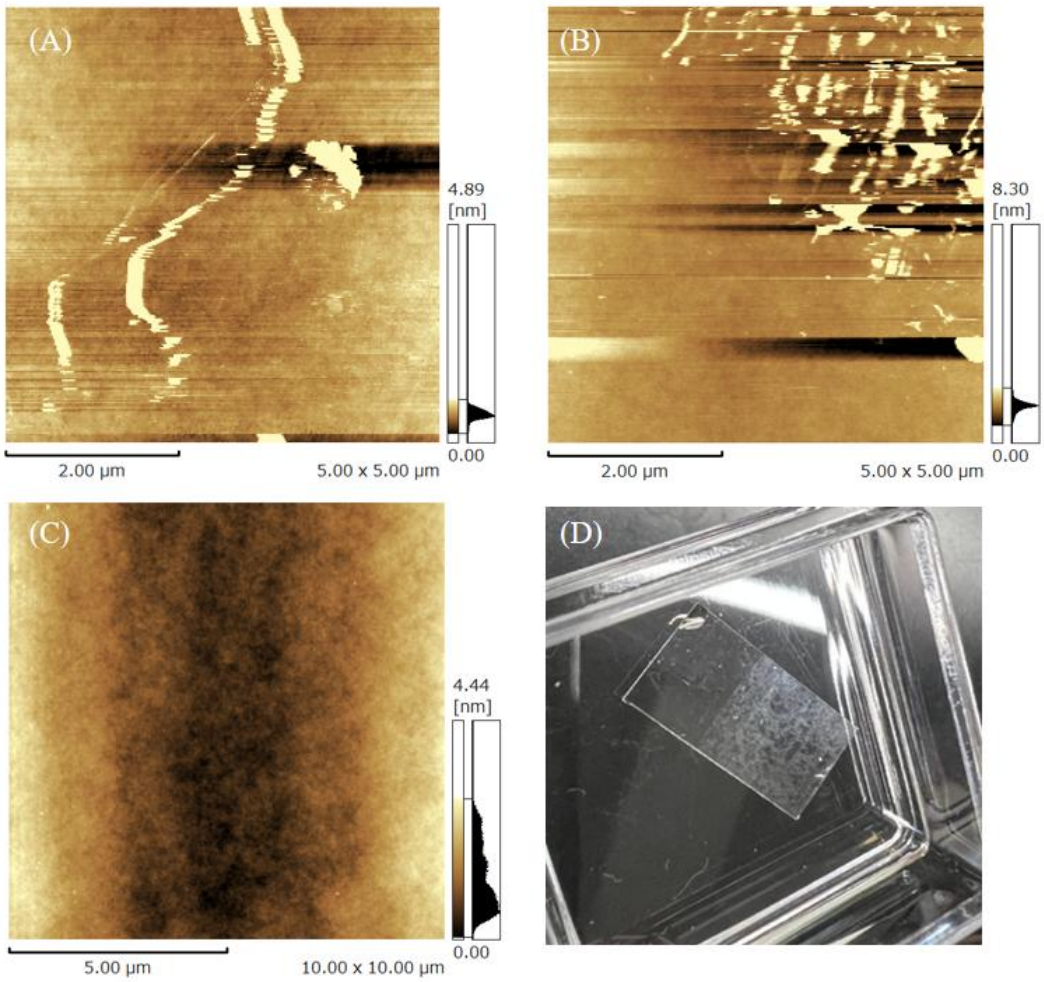

Fig. 4.10 AFM images of (A-B) POSS-1 transferred at a surface pressure of 40 mN/m, and (C) pure glass substrate without POSS transfer. (D) Photograph of POSS-1 transferred onto a glass substrate at a surface pressure of 40 mN/m.

Fig. 4.10 (A) and **(B)** show AFM images of two different regions of the same sample. Since the contact mode is used, the images show numerous artefacts related to lose surface-adsorbed particles. In cases where there is a weakly-bound molecular cluster on the surface and the cluster has significant height, the scanning tip may push the clusters on the surface, especially if the AFM feedback is too slow or the scan rate too high. This phenomenon can be observed in **Fig. 4.10 (A)**, where the two vertical bright bands are due to two clusters formed by 3D aggregation of POSS-1 that are being pushed on the surface by the probe's movement.

In **Fig. 4.10 (D)**, the roughness of the transferred film can be visually observed. Such surface roughness is not visible in the transferred films of the second and third categories of POSSs. To provide evidence for the formation of high islands by POSS-1, indicating 3D aggregation, height measurements were conducted on the AFM image, as illustrated in **Fig. 4.11**.

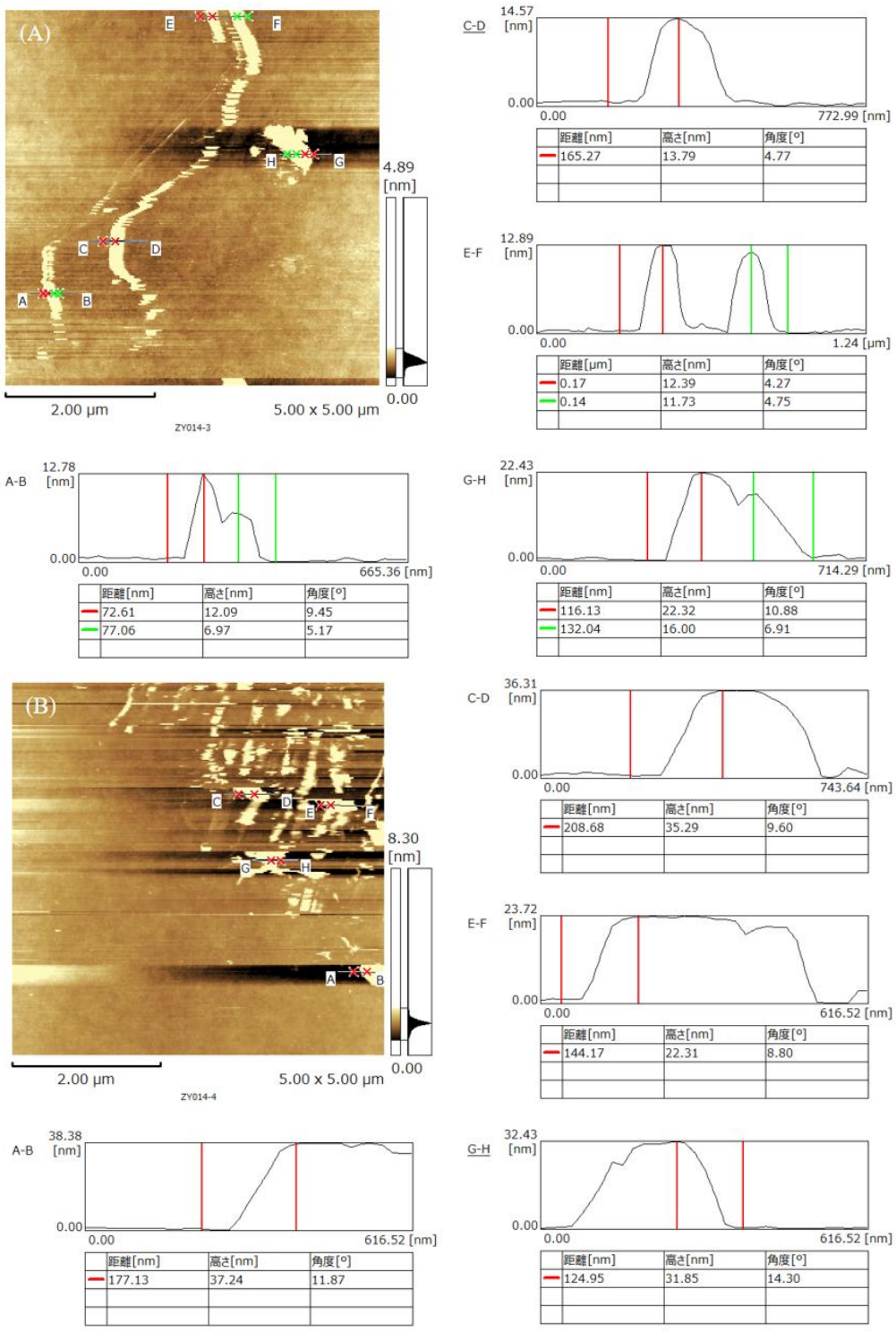

Fig. 4.11 AFM height measurement of POSS-1 transferred at a surface pressure of 40 mN/m.

The molecular diameter of POSS-1 estimated by Chem3D is only 0.95 nm. The analysis reveals that islands formed by POSS molecules with hydrophobic substituents due to 3D aggregation exhibit remarkably large heights that are several tens of times larger than their molecular size. No monolayer formation was observed.

For the second category of POSSs, except for the π-A isotherm of POSS-7 showing too low surface pressure in the transition state, the other three exhibited suitable curves for transfer.

According to their respective π-A isotherms, three different stages were selected for each POSS to transfer: before, during, and after the transition state, followed by AFM measurements. Firstly, **Fig. 4.12** shows the AFM images of POSS-6.

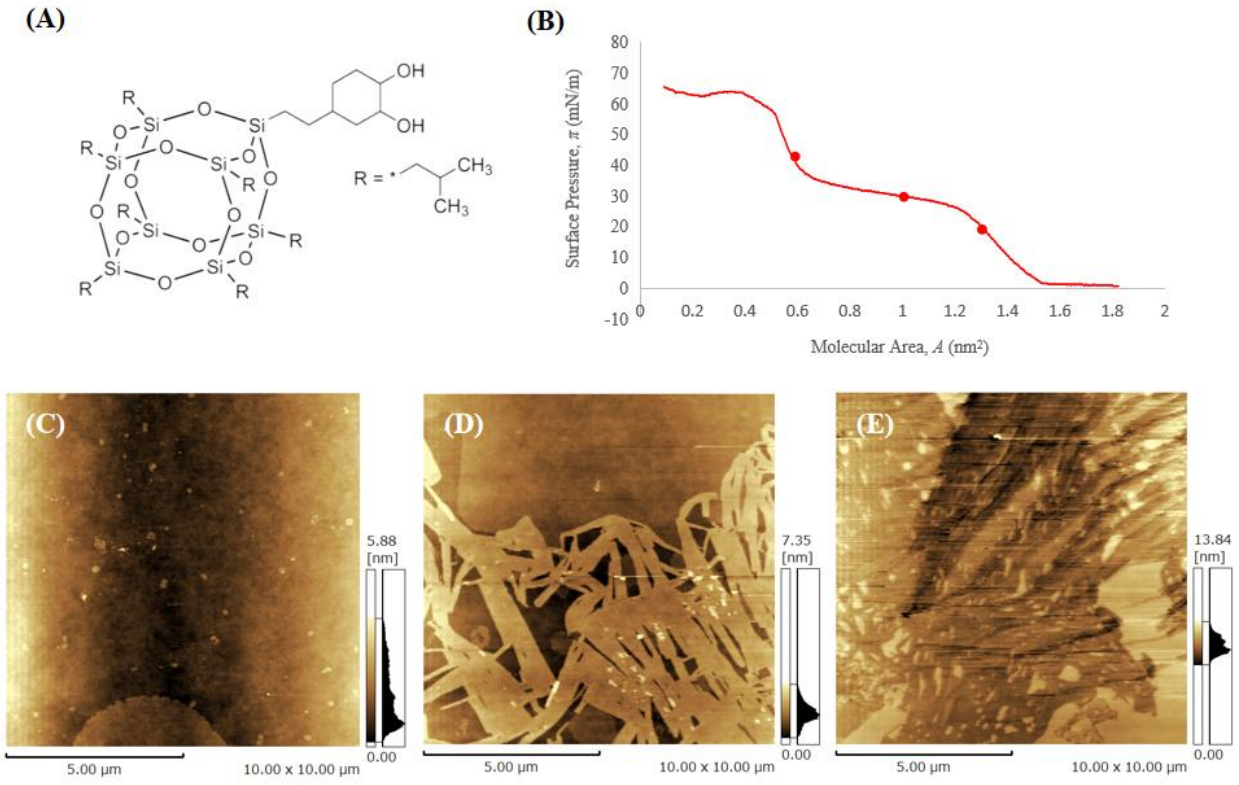

Fig. 4.12 (A) Molecular structure and (B) π-A isotherm of POSS-6, and its AFM images obtained after transferred at the surface pressure of (C) 20 mN/m, (D) 30 mN/m, (E) 40 mN/m.

In **Fig. 4.12 (C)** and **(D)**, more detailed images were obtained, enabling further height measurements. **Fig. 4.12 (E)** shows noticeable streaks in the image due to the AFM tip hitting surface clusters, indicating that molecular stacking occurs due to the small compressed area at this point. This image suggests that the surface of the substrate is almost completely covered by POSS molecules, making it challenging to determine the height of the first monolayer accurately. Therefore, this region was not subjected to further analysis.

In the AFM image of **Fig. 4.13**, at a surface pressure of 20 mN/m, a large region resembling a monolayer can be observed below, accompanied by scattered small regions appearing above. The height differences between these regions and the substrate surface are about 1.2 nm. Considering that its long-chain substituents undergo folding to change orientation after transfer, this approximates the single molecular size of 1.69 nm estimated with Chem3D. Based on this observation, it can be concluded that at this stage, the molecules have formed 2D assembly. The large-area monolayer formation is a result of small-area monolayers coming into proximity with each other, thereby contributing to the overall structure.

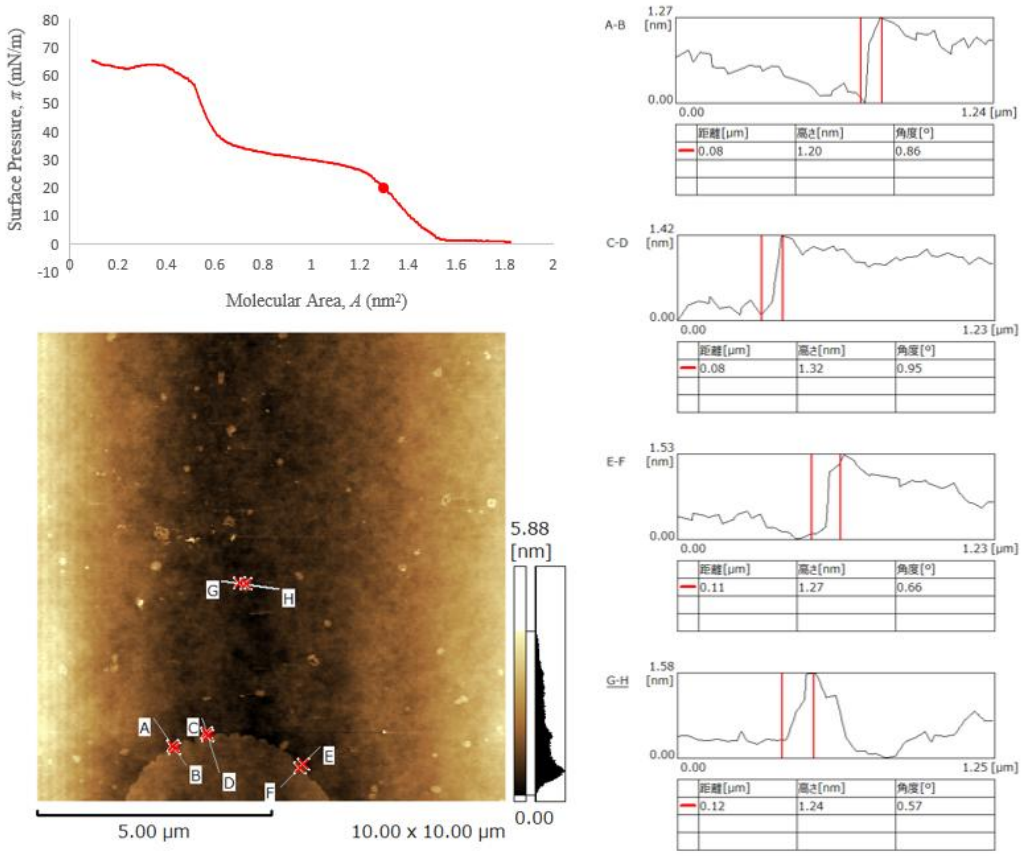

Fig. 4.13 AFM height measurement of POSS-6 transferred at a surface pressure of 20 mN/m.

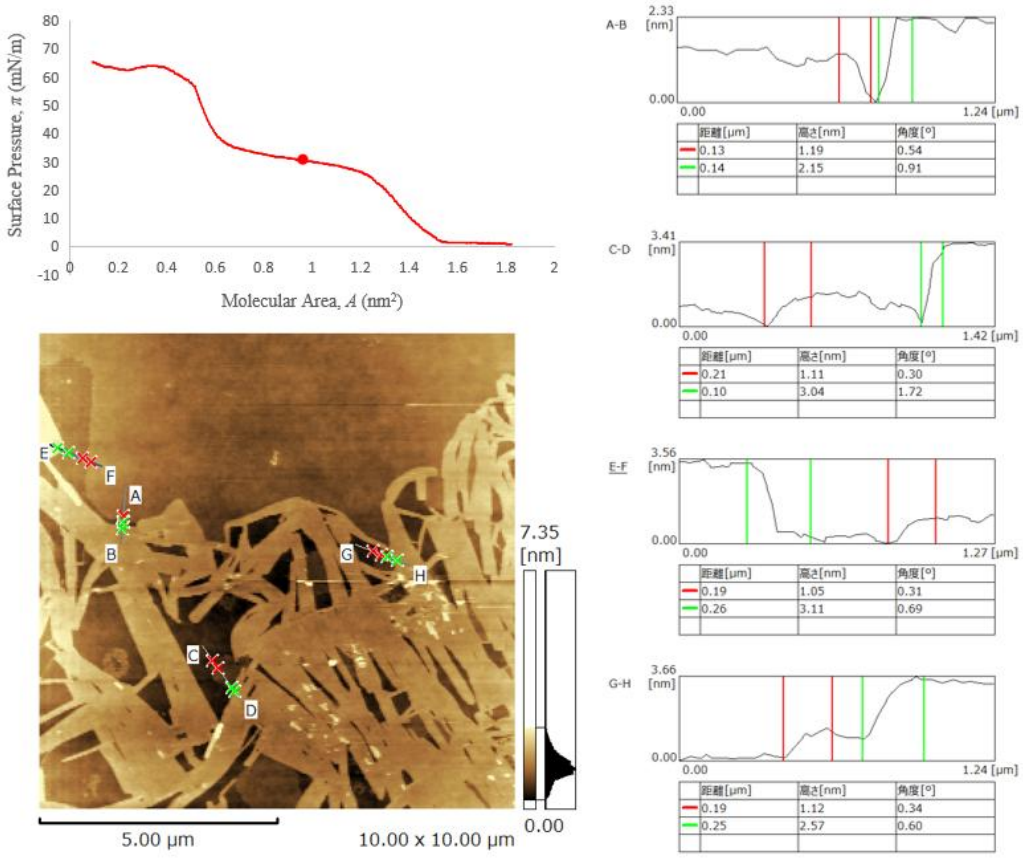

Fig. 4.14 AFM height measurement of POSS-6 transferred at a surface pressure of 30 mN/m.

Fig. 4.14 shows the AFM image of POSS-6 transferred at a higher surface pressure (30 mN/m)

compared to **Fig. 4.13**. By analyzing the height measurements, it can be seen that the height of certain regions is still around 1.2 nm, and the difference is within the error margin of AFM height measurement, which is consistent with the height difference shown in **Fig. 4.13**. This implies that with further compression, more small-area monolayers coverage to form a large-area monolayer. Concurrently, long band-like structures with a height of about 2-3 nm and a width of about 0.3 μm were also observed. They are uniform in height and width, and these structures may be bilayers or multilayers resulting from monolayer folding after the surface pressure exceeds the initial monolayer formation pressure. The 2D assembly of POSS occurs during the initial stage of compression until the early transitional phase, and the LB film at this time has a uniform morphology. Further compression would randomly collapse the LB film, leading to the formation of 3D aggregates, which is inconsistent with the experimental purpose.

Then there are AFM images of POSS-8, also transferred in three different stages. Notably, for this particular POSS, under the same surface pressure, two different surface morphologies were observed, as shown in **Fig. 4.15**.

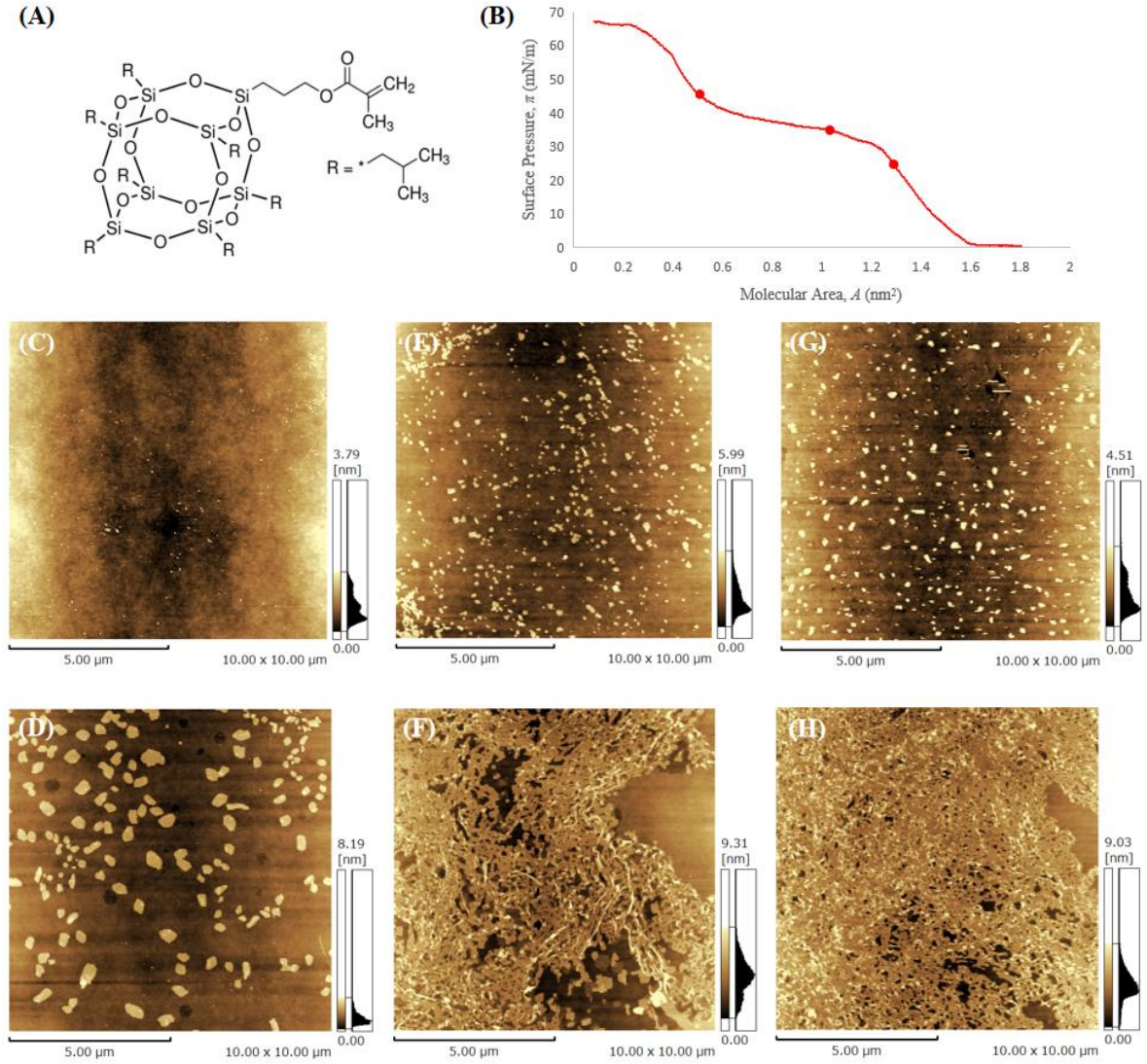

Fig. 4.15 (A) Molecular structure and (B) *π-A* isotherm of POSS-8, and its AFM images obtained

after transferred at the surface pressure of (C-D) 25 mN/m, (E-F) 35 mN/m, (G-H) 45 mN/m. Among them, (C), (E), (G) are obtained at the side of the sample, and (D), (F), (H) are obtained at the center of the sample.

As shown in **Fig. 4.15 (C)**, **(E)** and **(G)**, the AFM images obtained by measuring the side of the sample obtained scattered island-like distribution. The reason is that during the transfer process, the sides of the substrate contact the water meniscus, leaving dense deposit around the periphery. As shown in **Fig. 4.16**, it can be observed from the height measurements that the heights of the islands are in the range of 2-5 nm, much larger than the molecular size of 1.65 nm estimated by Chem3D. The side predominantly exhibits dispersed 3D aggregates, and the higher the surface pressure, the larger the islands formed.

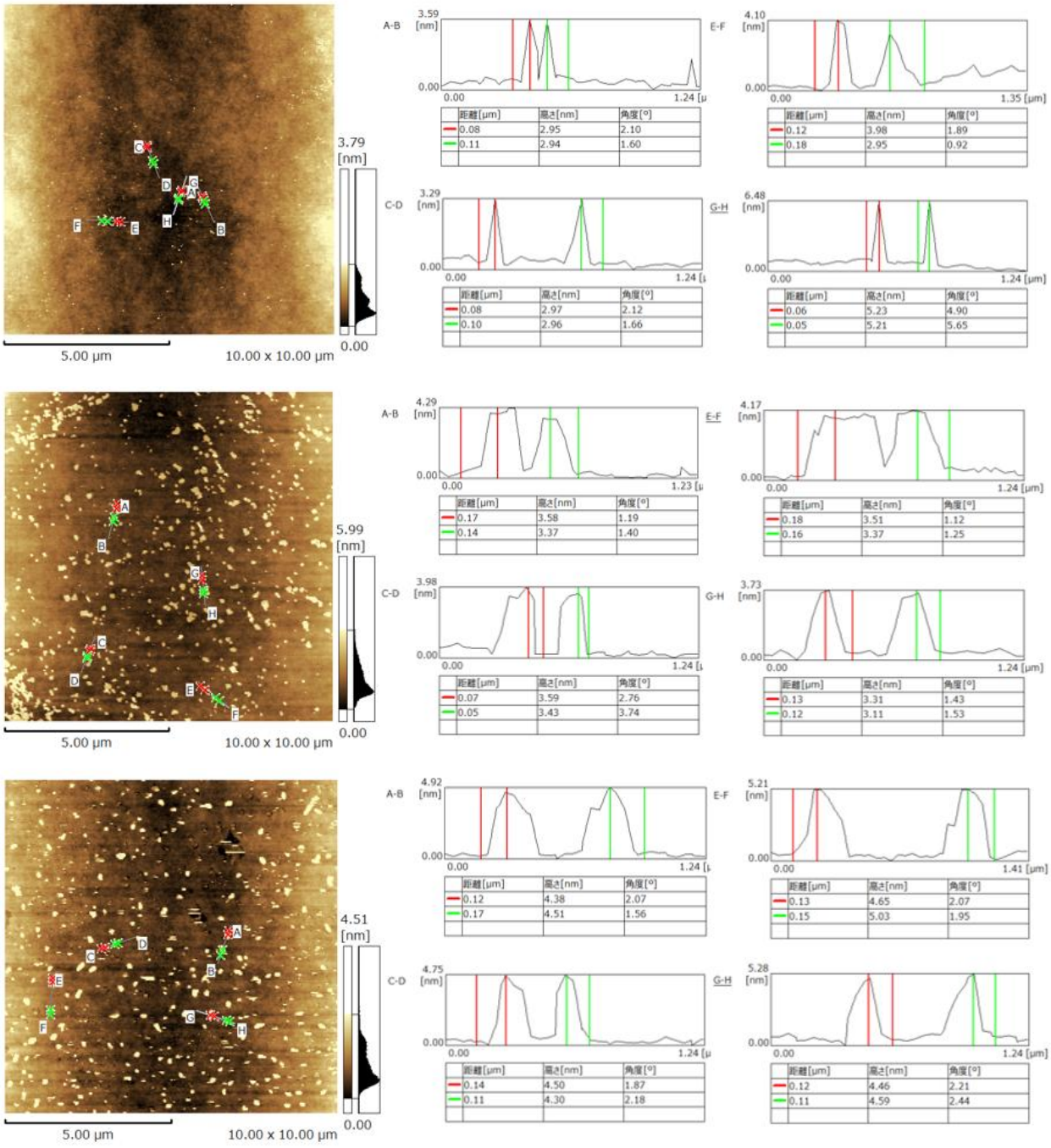

Fig. 4.16 From top to bottom, AFM height measurements at the sides of samples obtained after POSS-8 transferred at surface pressures of 25 mN/m, 35 mN/m, and 45 mN/m, respectively.

The AFM images obtained at the central region of the sample present compelling features that merit deeper investigation. At high surface pressure, due to the intermolecular interactions of POSSs, the islands in **Fig. 4.15 (D)** aggregated together by compression to form floc-like structures as shown in **Fig. 4.15 (F)** and **(H)**. To elucidate whether the amphiphilic POSS molecules assembled into a 2D structure during the initial stage of the π-*A* isotherm, height measurements were performed on **Fig. 4.15 (D)**, as shown in **Fig. 4.17**.

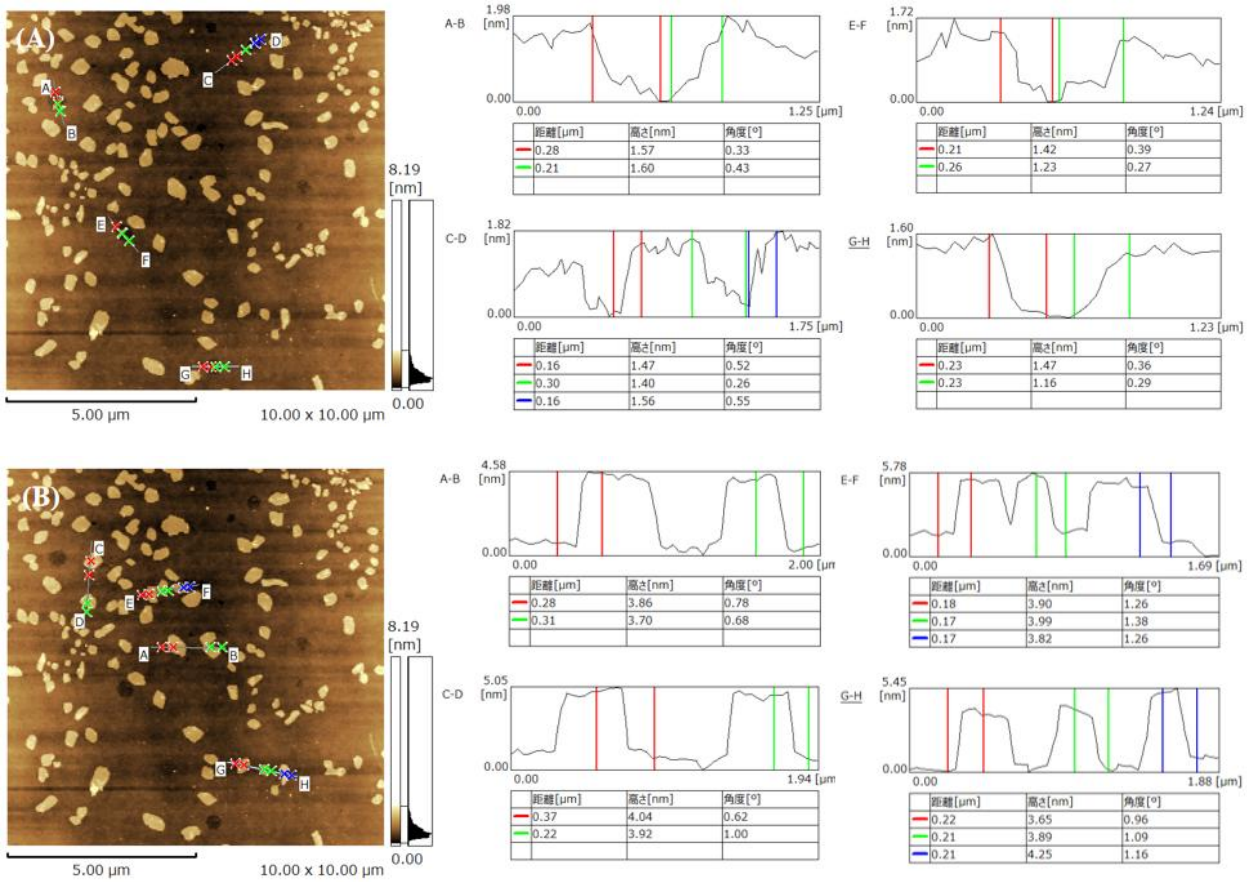

Fig. 4.17 AFM height measurements at the center of sample obtained after POSS-8 transferred at surface pressures of 25 mN/m. (A) shows the depth measurements of the holes and (B) shows the height measurements of the islands.

Analyzing the height data from **Fig. 4.17 (A)** indicates that the depth of the holes falls within the range of 1-2 nm, which corresponds to the molecular size of POSS-8 of 1.65 nm. This conformity suggests the formation of nearly uniform large-area monolayer, providing compelling evidence for the occurrence of 2D assembly during the early stages of the compression process. On the other hand, the height data reflected in **Fig. 4.17 (B)** demonstrates the 3D aggregation of POSS, with the measured height of the islands being approximately 3-4 times the molecular diameter. This

difference indicates a significant structural transition from 2D assembly to 3D assembly as the POSS molecules aggregate and form higher structures. With increasing surface pressure, multilayers may potentially form.

Finally, the third category of POSS was subjected to transfer and AFM measurements despite its low surface pressure exhibited by the *π-A* isotherm. The two selected surface pressures for the transfer were before the transition state and during the transition state, as shown in **Fig. 4.18**.

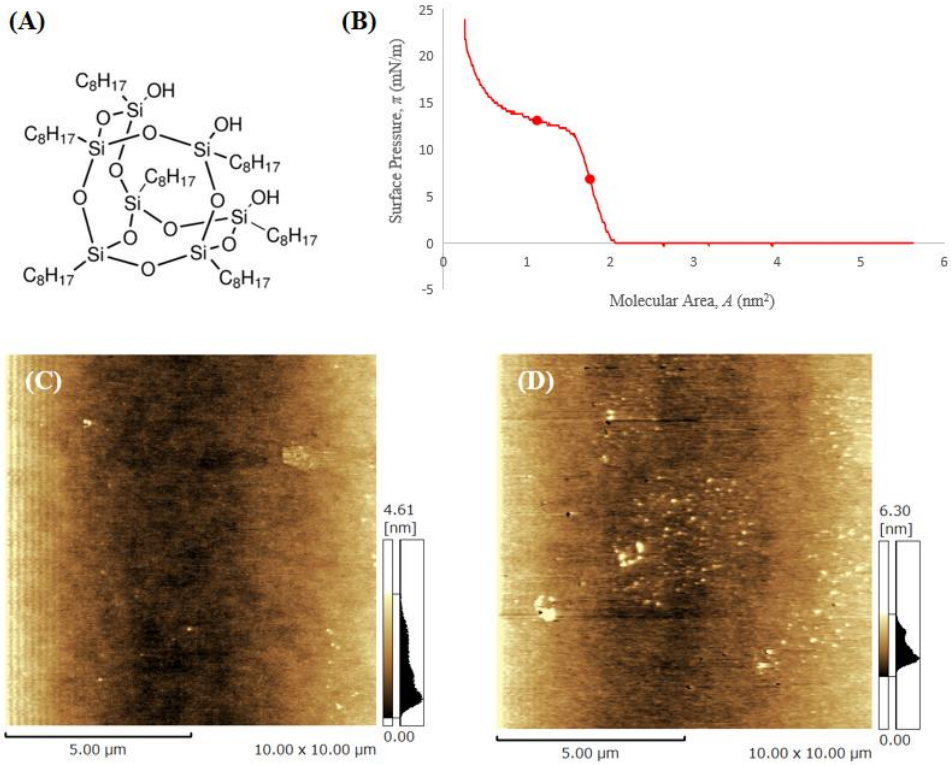

Fig. 4.18 (A) Molecular structure and (B) *π-A* isotherm of POSS-9, and its AFM images obtained after transferred at the surface pressure of (C) 6 mN/m and (D) 13 mN/m.

It can be observed from the AFM images that only a small number of molecules were transferred onto the substrate. This may be due to the larger volume of this IC-POSS compared with other POSSs, in order to obtain a more complete *π-A* isotherm, the number of molecules spread during the compression stage is very small, resulting in the formation of relatively sparse Langmuir film at the interface. In this case, to achieve a monolayer of this IC-POSS, more molecules need to be added to provide a sufficient molecular density. However, this contradicts the low surface coverage density required for the *π-A* isotherm. Another possibility is that because POSS-9 has hydroxyl groups, the molecules formed hydrogen bonds through the hydroxyl groups toward each other, and then formed dimers, stacking on top of the monolayer, as shown in **Fig. 4.19** [47]. Hydrophobic groups are exposed on the surface of the dimers. After further compression, they self-assembled into non-equilibrium crystal structures through van der Waals forces. Therefore, the dimers of POSS-9 are difficult to attach to the hydrophilic glass surface.

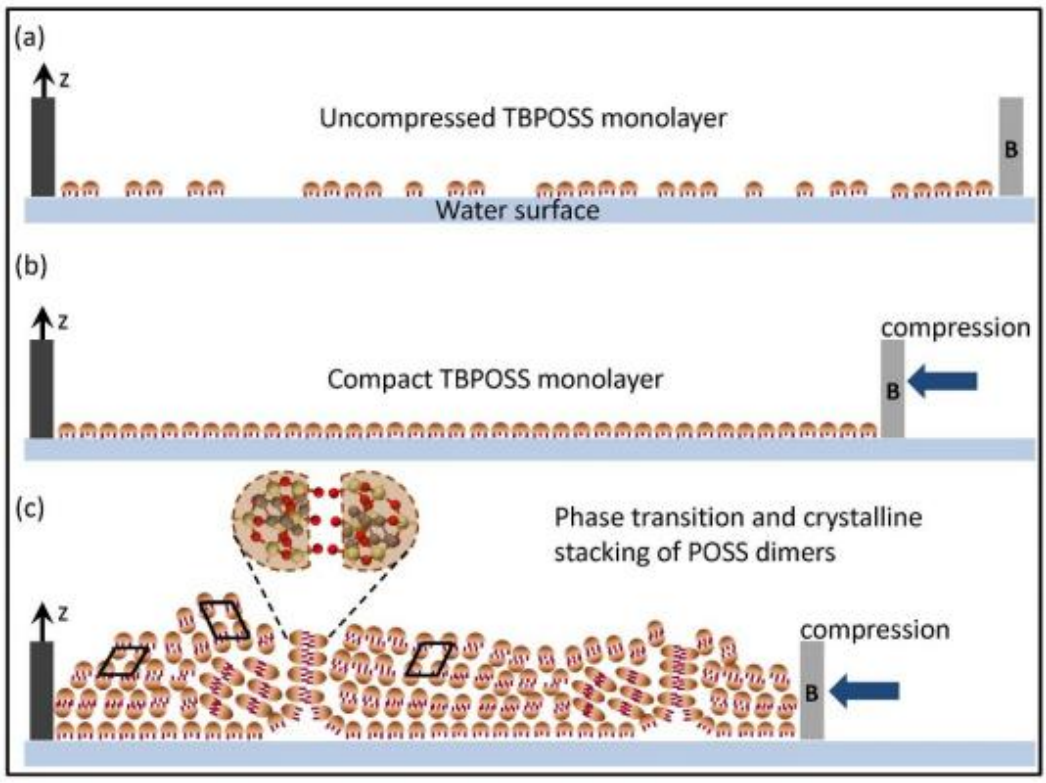

Fig. 4.19 Schematic illustration of the mechanism of reversible meta-stable transition of TBPOSS molecules from monolayer phase to crystalline phase by stacking of molecular dimers as a function of lateral pressure. (a) TBPOSS monolayer before compression and (b) after 1st compression which leads to compact monolayer. (c) Further compression leads to a phase transition to crystalline phases wherein the molecular dimers form crystalline stacks over the monolayer. [47]

In summary, the transferred films of POSSs were analyzed by AFM measurements. The first category of hydrophobic POSS molecules aggregated with each other and stacked to form highly random 3D aggregates, with no observed monolayer formation. For the second category of POSSs with hydrophilic substituents, the measured heights of the films transferred in the early transition state matched the molecular sizes, demonstrating that the amphiphilic POSSs achieved 2D assembly. Further compression resulted in a somewhat uniform 3D assembly above the monolayer. The morphology of the 3D assembly varies due to the properties of the POSS molecules themselves. For the third category of POSS, only a small number of molecules were transferred to the substrate, which may be due to the low number of molecules at the interface or the formation of dimers of IC-POSS.

Chapter 5

Conclusions

In this thesis, the LB method was used to manipulate the arrangement of POSS molecules at the air-water interface, allowing for a controlled assembly process. Using the LB system manufactured by our own laboratory and the commercial LB systems at NIMS, and comparing the π-A isotherms results obtained with several different LB systems, it was shown that the performance of the LB systems constructed in our lab was equivalent to the commercial LB systems at NIMS. The experimental LB system was improved to achieve larger trough size and slower compression speed, giving molecules more space and time to rearrange and adsorb, thus forming a more uniform monolayer.

By adjusting parameters such as the solution volume, the π-A isotherms of three categories of POSS molecules were obtained, and the assembly behaviors of hydrophobic POSS, amphiphilic POSS and IC-POSS were analyzed according to the isotherms. Due to the hydrophobic core of POSS, the molecules tend to form random 3D aggregates at the interface. The presence of hydrophilic substituents endows amphiphilic properties to the molecules, enabling 2D assembly. Using Chem3D to model the various POSS molecules, the cross-sectional area of each POSS derivative was calculated from the obtained molecular diameter. Comparing this value with the molecular area A_0 where the surface pressure rises above zero demonstrates the 2D assembly of amphiphilic POSS molecules at the interface. As for IC-POSS, its cross-sectional area estimation has a wide range, making it difficult to compare with the A_0 value. Furthermore, although it exhibited a lower surface pressure in the π-A isotherm, it also showed a transition state, possibly implying the formation of dimers.

According to the respective π-A isotherms, different stages were chosen to transfer POSS thin films to glass substrates under multiple surface pressures by the LB method. The transferred material was then characterized using AFM. Hydrophobic POSS molecules aggregated and stacked on top of each other to form highly random 3D aggregates, and no monolayer formation was observed. For the amphiphilic POSS, the measured height of the film transferred in the early transition state matched the molecular size, proving that POSS achieved 2D assembly. Further compression resulted in a somewhat uniform 3D assembly above the monolayer. The morphology of the 3D assembly varies due to the properties of the POSS molecules themselves. For IC-POSS, only a small number of molecules were transferred onto the substrate, which may be due to the low number of molecules at the interface or the formation of dimers. Therefore, the LB method is not suitable to achieve 2D assembly of IC-POSS.

Preparing POSS as 2D materials has the advantage of expanding its potential applications.

However, LB technique for POSSs was found to have some challenges, such as poor control over uniformity and consistency in the preparation of large-area thin films, as well as the requirements for reactive functional groups and surface activity of amphiphilic POSS molecules. In summary, this study provides an approach to fabricating POSS LB films and provides an overview of the layer-forming properties of POSS, offering an ordered and oriented material platform for future applications such as constructing chemical sensors. The broader applications of POSS in the field of materials science are worth exploring.

References

[1] H. Zhang, *ACS Nano.* **9**, 9451 (2015).

[2] Y. Liu, N. Weiss, X. Duan, *et al. Nat Rev Mater* **1**, 16042 (2016).

[3] K. S. Novoselov, A. K. Geim, S. V. Morozov, *et al*. *Science* **306**, 666 (2004).

[4] J. Hass, R. Feng, T. Li, *et al*. *Appl. Phys. Lett* **89**,143106 (2006).

[5] X. Y. Yang, X. Dou, A. Rouhanipour, *et al*. *J. Am. Chem. Soc.* **13**, 130 (2008).

[6] K. S. Novoselov, D. Jiang, T. Booth, *et al*. *Proc. Natl. Acad. Sci. USA* **102**, 10451 (2005).

[7] K. F. Mak, C. Lee, J. Hone, *et al*. *Phys Rev Lett*. **105**, 136805 (2010).

[8] F. Bonaccorso, L. Colombo, G. Yu, *et al*. *Science* **347**,1246501 (2015).

[9] J. Albero, D. Mateo, H. Garcia, *Molecules* **24**, 906 (2019).

[10] X. Sun, Z. Liu, K. Welsher, *et al*. *Nano Research* **1**, 203 (2008).

[11] S. Kim, M. Lippmaa, J. Lee, *et al*. *Adv. Mater. Interfaces* **9**, 2201781 (2022).

[12] D. Khim, A. Luzio, G. E. Bonacchini, *et al*. *Adv. Mater.* **30**, 1705463 (2018).

[13] M. Chhowalla, H. Shin, G. Eda, *et al. Nat. Chem.* **5**, 263 (2013).

[14] J. R. Smith, A. B. Johnson, *J. Mater. Chem.* **45**, 789 (2022).

[15] T. Sawada, A. Yamamura, M. Sasaki, *et al*. *Nat. Commun.* **11**, 4839 (2020).

[16] Y. Li, W. Hu, Y. Li, *et al*. *Adv. Mater.* **29**, 1605590 (2017).

[17] Y. Zhang, J. Liu, C. Qi, *J. Mater. Sci*. **53**, 2307 (2018).

[18] J. Smith, A. Johnson, *J. Mater. Sci*. **45**, 567 (2022).

[19] J. Wang, S. S. A. Zaidi, A. Hasnain, *et al*. *ACS Biomater. Sci. Eng.* **4**, 2155 (2018).

[20] Nicholas K. Kildahl, *J. Chem. Educ.* **72**, 423 (1995).

[21] K. Tanaka, Y. Chujo, *Polym. J* **45**, 247 (2013).

[22] F. A. Sheikh, N. A. M. Barakat, B. S. Kim, *Mat. Sci. Eng. C-Bio*. **29**, 869 (2009).

[23] M. Gon, S. Saotome, K. Tanaka, *et al*. *ACS Appl. Mater. Interfaces.* **13**, 12483 (2021).

[24] W. Li, H. Li, C. Zeng, *et al*. *Chem. J. Chinese Universities*, **43**, 20210629 (2022).

[25] M. A. Nabhan, C. A. S. Batista, D. E. Cliffel, *et al*. *ACS Appl. Polym. Mater.* **5**, 3278 (2023).

[26] T. Alphazan, L. Mathey, M. Schwarzwälder, *et al. Chem. Mater.* **28**, 3634 (2016).

[27] S. Samanta, S. Sarkar, N. K. Singha, *ACS Appl. Mater. Interfaces.* **15**, 24812 (2023).

[28] Z. Niu, G. Li, X. Ma, *et al*. *COMPOS PART A-APPL S.* **155**, 106855 (2022).

[29] I. Jerman, A. Š. Vuk, M. Koželj, *et al*. *Langmuir* **24**, 5029 (2008).

[30] X. Xu, Y. Shao, W. Wang, *et al*. *Langmuir* **37**, 4294 (2021).

[31] K. B. Blodgett, *J. Am. Chem. Soc.* **57**, 1007 (1935).

[32] A. Blume, *ChemTexts* **4**, 3 (2018).

[33] D. R. Talham, *Chem. Rev.* **104**, 5479 (2004).

[34] M. Chikazawa, K. Tajima, 界面化学 (丸善出版, 2001).

[35] M. Hitrik, V. Gutkin, O. Lev, *et al*. *Langmuir* **27**, 11889 (2011).
[36] A. W. Adamson, A. P. Gast, *Physical chemistry of surfaces*, 6th edn. Wiley, New York (1997).
[37] H. Möhwald, *Annu. Rev. Phys. Chem.* **41**, 441 (1990).
[38] V. M. Kaganer, H. Möhwald, P. Dutta, *Rev. Mod. Phys.* **71**, 779 (1999).
[39] K. Y. C. Lee, *Annu Rev Phys Chem* **59**, 771 (2008).
[40] G. L. Gaines, *Wiley Interscience, New York* (1966).
[41] K. Sakakibara, T. Fujisawa, J. P. Hill, *et al*. *Phys. Chem. Chem. Phys.* **16**, 10286 (2014).
[42] P. Bertoncello, A. Notargiacomo, C. Nicolini, *Langmuir* **21**, 172 (2004).
[43] F. J. Feher, T. A. Budzichowski, R. L. Blanski, *et al*. *Organometallics*. **10**, 2526 (1991).
[44] F. J. Feher, R. Terroba, J. W. Ziller, *Chem Commun*. **35**, 2309 (1999).
[45] T. Uchihashi, Atomic force microscopy, KoubunnshiGakkai-webpage: https://www.spsj.or.jp/equipment/news/news_detail_22.html: 2023/5/30
[46] N. Jalarvo, O. Gourdon, G. Ehlers, *et al. J. Phys. Chem. C* **118**, 5579 (2014).
[47] R. Banerjee, M. Sanyal, M. Bera, *et al*. *Sci Rep* **5**, 8497 (2015).

Acknowledgement

First of all, I would like to express my deepest gratitude to my supervisor, Prof. Mikk Lippmaa, for his unwavering support and patient guidance throughout the entire research and thesis writing process. Although my research direction is not the same as that of most members in the lab, he never refused my attempt. Professor Lippmaa always approaches research with enthusiasm, and I have often gained new knowledge from our discussions. His expertise and insights have been crucial to my work, and I feel honored to have studied in his group for two years.

Secondly, I would like to express my gratitude to Dr. Taizo Mori. He has a deeper understanding of my research field and has been of tremendous help to me throughout my research and thesis writing process. Although he was very busy with his experiments, whenever I encountered difficulties, he always gave me valuable advice and took time to accompany me to find solutions.

I would also like to thank all other present and graduated members of Lippmaa lab during my research years, Ms. Junko Nagayama, Ms. Hanako Kuramochi, Ms. Jiayue Ma, Mr. Tetsuhiro Hattori, Mr. Jiwon Yang, Ms. Sarah Tobisch, Mr. Haotong Liang, and Mr. Yunlong Sun. It is because of your support and companionship that I was able to have a fulfilling time during my master's studies.

Finally, I would like to thank my family, Weijie Zhang and Xiaolu Sun. Thank you for encouraging me to pursue my dream in a foreign land and for providing me with financial support for studying abroad.

July 2023

Yuchen Zhang